Geochemical Characteristics and Environmental Implications of the Paleocene-Eocene in the Jiangling Depression, Southwestern Jianghan Basin

Kai Yan , Chunlian Wang * , Renyi Chen , Jiuyi Wang , Ruiqin Li , Lihong Liu

Posted Date: 8 November 2023

doi: 10.20944/preprints202311.0490.v1

Keywords: Jiangling depression; Paleocene-Eocene saline lake; climate; redox conditions; salinity

Article

Geochemical Characteristics and Environmental Implications of the Paleocene-Eocene in the Jiangling Depression, Southwestern Jianghan Basin

Kai Yan [1,2], Chunlian Wang [1,*], Renyi Chen [1], Jiuyi Wang [1], Rui-qin Li [3,4] and Li-hong Liu [3,5]

[1] MNR Key Laboratory of Metallogeny and Mineral Assessment, Institute of Mineral Resources, Chinese Academy of Geological Sciences, Beijing 100037, China
[2] Institute of Earth Sciences, University of Iceland, Sturlugata 7, 102 Reykjavík, Iceland
[3] School of earth and space Sciences, Peking University, Beijing 100871, China
[4] Department of Geological Sciences and Environmental Studies, State University of New York at Binghamton, New York, 13902, USA
[5] Oil & Gas Survey, China Geological Survey, Beijing 100083, China
* Correspondence: should be addressed to Chunlian Wang; wangchunlian312@163.com

Abstract: This research investigates the environmental characteristics of the saline lake in the Jiangling depression, southwestern Jianghan Basin from Paleocene to Eocene using bulk-rock geochemistry. The ratios of FeO/MnO, Al_2O_3/MgO and C-value indicate a semi-humid to semi-arid climate in the early-middle Paleocene. There was a rapid shift to a humid climate during the late Paleocene to early Eocene, following a short-time intense dryness. The Eocene climate was arid, but experienced intermittent humidity. The variation trend of CIA, CIW and PIA is similar to that of FeO/MnO, Al_2O_3/MgO and C-value, so the chemical weathering was influenced by climate changes. The redox conditions of lake in the Jiangling depression during Paleocene to Eocene were reconstructed using the ratios of U/Th, Ni/Co, and V/Cr. In the humidity and alternations of aridity and humidity, the lake water received external water input, resulting in weak stratification, so the sediments were in oxidation condition. In the aridity, lakes become a still water environments, leading to sediments formed in reduced condition. The salinity of the lake in Jiangling depression from Paleocene to Eocene was determined through the analysis of sedimentary sequences and the change of Sr/Ba ratio. In the early-middle Paleocene, the salinity of lake varied greatly. From the late Paleocene to the early Eocene, the salinity of lake decreased. In the Eocene, the salinity of the lake increased, and the halite precipitated, and finally the salinity of the lake decreased due to humid climate.

Keywords: Jiangling depression; Paleocene-Eocene saline lake; climate; redox conditions; salinity

1. Introduction

The Jianghan Basin is a Mesozoic-Cenozoic rift basin in central China, which has experienced multi-stage tectonic movement. In the Paleocene, the Jianghan Basin deposited abundant evaporites, and potassium and lithium-rich brine ore (Wang et al., 2013, 2021; Liu, 2013; Shen et al., 2014; Liu et al., 2015). In view of the sedimentary characteristics of evaporite in a series of rifted basins in south China, Liu et al. (2013, 2016) proposed that the formation of evaporite deposits was controlled by tectonics, provenance and climate. This is because some scholars once believed that Jianghan Basin was affected by the subtropical highs controlled by the planetary wind system during the Late Cretaceous-Early Paleogene, and the climate was mainly hot and arid (Sun and Wang, 2005; Guo et al., 2008). However, with the discovery of PETM, there is evidence that the precipitation in Jianghan Basin increased significantly during the Early Paleogene, and the climate was mainly warm and humid (Teng et al., 2021; Xie et al., 2022; Yan et al., 2022). The latest research results challenge the view that evaporite was formed in arid climate environment, so it is urgent for us to carry out more detailed research on evaporite strata in the Jiangling depression, southwestern Jianghan Basin to determine the paleoenvironment and paleoclimate at that time.

 doi:10.20944/preprints202311.0490.v1

At present, there are many researches on the climate and environment characteristics of the early Paleogene in the Jiangling depression, but there are great differences due to the experimental objects and methods. The analysis of palynological types shows that the climate in Jianghan Basin was subtropical arid during Paleocene, and alternating between humid and arid in Eocene (Sun and Wang, 2005; Wang et al., 2020). And Wang et al. (2013) revealed the change of paleoclimate conditions from hot and arid Paleocene to humid Eocene in the Jiangling depression by using the changes of carbon and oxygen isotope composition of carbonate in lacustrine sediments. However, Li et al. (2015, 2016), based on the fluid inclusion temperature test of anhydrite and halite, believed that the temperature in the early Eocene was between 14.9 and 38.5 ℃, which decreased compared with the Paleocene, but the climate was still mainly hot and arid. Therefore, we try to use different analysis and testing methods to study the Paleocene-Eocene climate and environmental characteristics of the Jiangling depression. After many years of development, geochemical parameters have been widely used in paleoenvironmental conditions, tectonic setting and clastic rock provenance (e.g., Nesbitt and Young, 1982; Bhatia, 1986; McLennan et al., 1995; Hetzel et al., 2011; Fang et al., 2023). And the composition of clastic sedimentary rocks is controlled by a combination of factors such as parent rock composition, weathering (physical and chemical), transport, sedimentation, and diagenesis (Johnsson, 1993). Therefore, geochemical data analysis can provide a reliable basis for reconstructing the paleoenvironment of evaporite sedimentary strata in the Jiangling depression.

2. Geological Setting

The Jianghan Basin located in the Yangtze Block of central China, is a large Mesozoic-Cenozoic rift basin, with a total area of 36,360 km^2 (Gilder et al., 1991; Yu et al., 2003; Teng et al., 2019). It is surrounded by various geological features, such as the Qinling orogen in the north, the Dabie Terrance in the northeast, the Edong fold-thrust belt in the east, the Jiangnan orogen in the south, and the Huangling massif and the Xiang'exi fold-thrust belt in the west (Hu et al., 2006; Shen et al., 2012; Li et al., 2015; Wu et al., 2017; Wang et al., 2022) (Figure 1A). The Presinian metamorphic basement of the Jianghan Basin was formed during the Late Proterozoic. The basement of the Jianghan Basin consists of two parts: the underlying crystalline basement and the overlying pre-rift strata. The crystalline basement of the Jianghan Basin mainly consists of Archean-Proterozoic metamorphic and metasedimentary rocks (Wu et al., 2017). During the Sinian to the Early Triassic, with the influence of the regional Indosinian movement spreading to this area, the Jianghan Basin uplifted to different degrees under the background of dramatic and rapid crustal rise, and the sea water slowly withdrew westward, forming a set of extensive coastal clastic rocks interbedded with Marine carbonate rocks (Dai et al., 1996; Yao et al., 2015). The Middle Triassic to Jurassic sediments in the Jianghan Basin were mainly terrestrial conglomerate, sandstone and mudstone, and interbedded with coal seams formed from Carboniferous to Early Triassic (Chen et al., 2013; Shu et al., 2008). Under the influence of the Yanshanian movement, a NW-trending fault belt was formed in the Jianghan Basin from Late Jurassic to Early Cretaceous (Hu et al., 2006). From the late Cretaceous to Paleogene, the Jianghan Basin experienced the active upwelling of the upper mantle induced by the rolling of the Pacific plate and the Indo-Asian collision, resulting in multi-stage rifting and the formation of extensive siliceous clasts, evaporites and a large number of basalts in the basin, and finally formed the present geographical characteristics (Liu et al., 2004; Li et al., 2015).

Preprints (www.preprints.org) | NOT PEER-REVIEWED | Posted: 8 November 2023 doi:10.20944/preprints202311.0490.v1

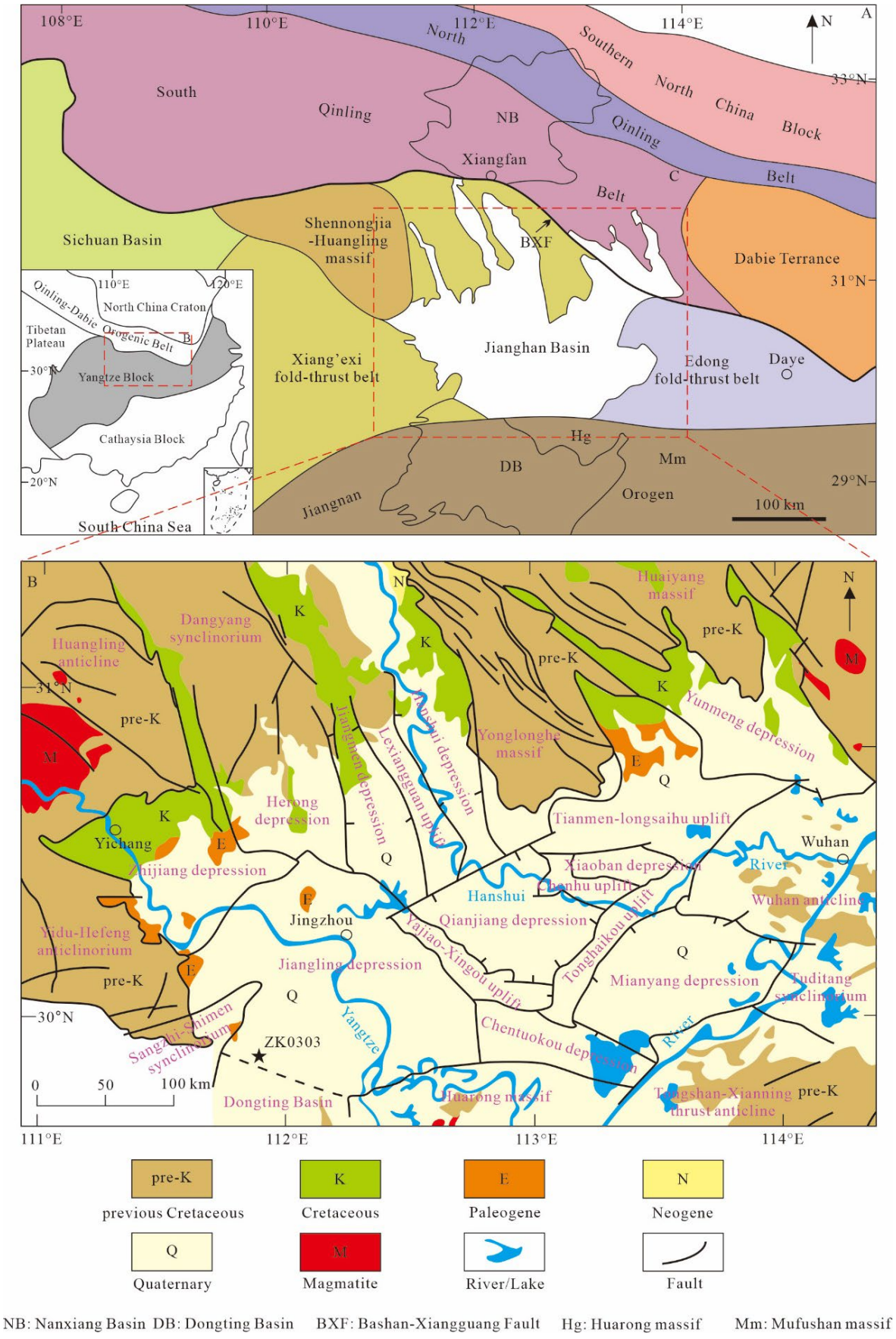

Figure 1. Geologic and tectonic sketch maps of the Jianghan Basin region. (A) modified after Chen et al., (2013).

Preprints (www.preprints.org) | NOT PEER-REVIEWED | Posted: 8 November 2023 doi:10.20944/preprints202311.0490.v1

The Jianghan Basin is composed of several secondary structural units and depressions. The Jiangling depression is the largest secondary negative tectonic unit in Jianghan Basin, which was formed on the Yanshanian fold basement under the depression setting of Late Cretaceous to Paleogene (Figure 1B). The growth and development of the Jiangling depression are controlled by Qingshuikou fault, Jishansi fault, Wen'ansi fault and Gongan-Songzi fault, and divided into two independent units by Wancheng fault (Wang et al., 2013; Yang et al., 2003; Yu et al., 2018) (Figure 2). In 2016, we obtained a 2,302.03 m long well (ZK0303) in the southwest of the Jiangling depression. The core is mainly composed of purplish pink silty mudstone and dark gray mudstone, interbedded with anhydrite, glauberite and halite. According to the existing palynological records and the stratigraphic correlation study of adjacent well, it is preliminarily believed that the boundary between Paleocene and Eocene is around 680 m of the drilling core (Yan et al., 2022).

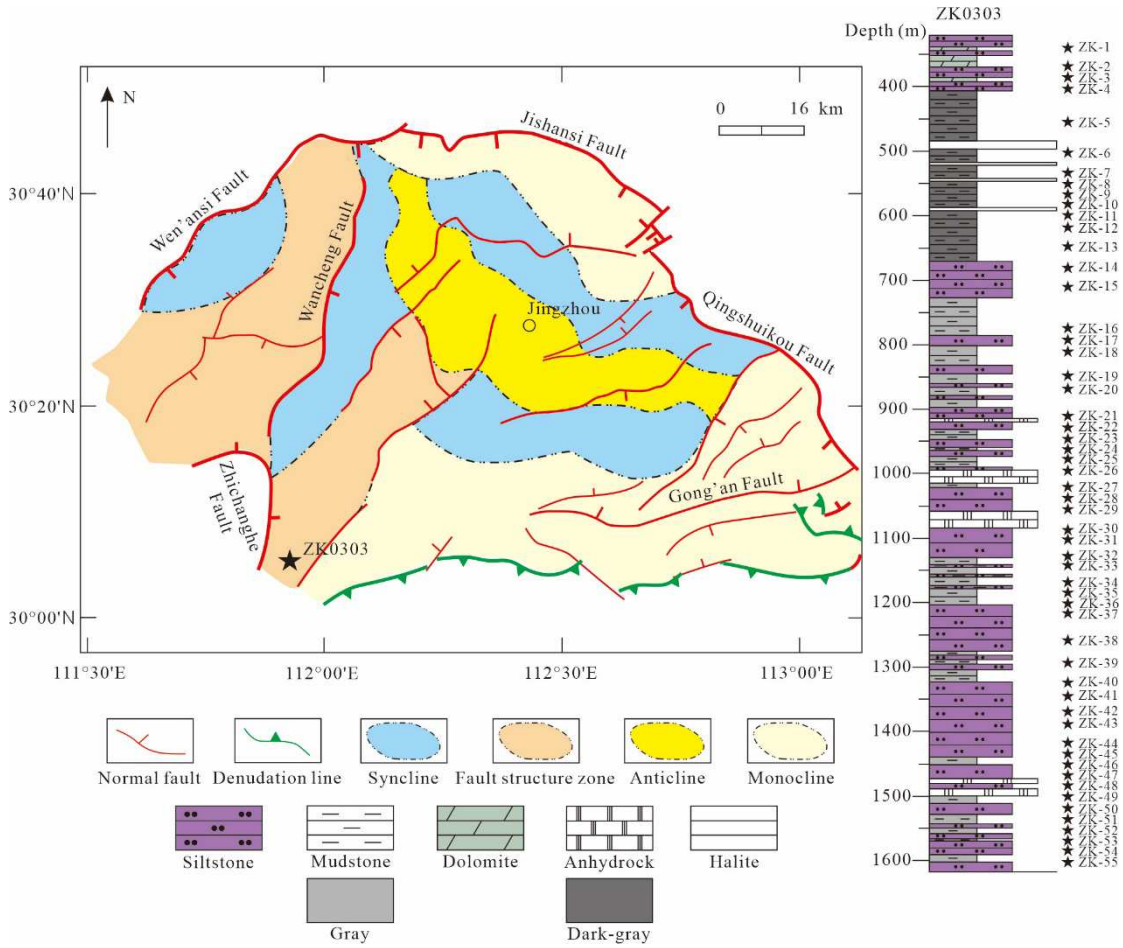

Figure 2. Tectonic map of the Jiangling depression (modified after Teng et al., 2019), and stratigraphic column of well ZK0303.

3. Sampling and Methods

A total of 55 samples were collected from Well ZK0303 based on the criteria of vertical differences, changes in sediment color, particle size and physical properties (Figure 2). We split the core ZK0303 into two halves in the longitudinal, and selected the fresh part that was not contaminated. All samples were stored in plastic bags to avoid secondary pollution and oxidation as much as possible. Before the geochemical analysis all samples were air-dried, crushed to 200 mesh and thoroughly mixed. The major elements were analyzed by X-ray fluorescence spectrometer (XRF), and the analytical accuracy was estimated at 1% for SiO2 and 2% for the other oxides. The trace and rare earth elements were tested by inductively coupled plasma mass spectrometry (ICP-MS), and the the analytical uncertainties were estimated at approximately 10% and 5% for trace and rare elements with abundances of <10 ppm and >10 ppm, respectively.

Preprints (www.preprints.org) | NOT PEER-REVIEWED | Posted: 8 November 2023 doi:10.20944/preprints202311.0490.v1

Before the experiment, the samples were crushed in an agate mortar to less than 200 mesh. After that, the powdered samples were heated and poured into the mixture of anhydrous lithium tetraborate, lithium fluoride and ammonium nitrate to melt into glass sheets, which were continued to be heated in a muffle furnace to determine loss on ignition. Finally, the fused samples were heated to 800°C and analyzed using a sequential X-ray fluorescence spectrometer (AB104L, Axios-mAX). Calibrations of accuracy and reproducibility were conducted using the GB/T 14506.14-2010 and GB/T 14506.28-2010 standards.

The content of trace and rare earth elements were measured by inductively coupled plasma mass spectrometer (ICP-MS, ELEMENT XR). Heat the powdered samples with HF and HNO_3. After evaporation to dryness, HNO_3 was added to dissolve the samples. Then, HNO_3 was added to samples again and heated to 130°C. Finally, the distilled water was added to the solution and the contents of trace elements were measured. All geochemical analyses were carried out in the Analytical Laboratory Beijing Research Institute of Uranium Geology.

4. Results

4.1. Major Elements Geochemistry

Among the major elements, the contents of SiO_2 (15.65-58.40 wt.%, average 44.22 wt.%), Al_2O_3 (4.14-17.58 wt.%, average 13.24 wt.%) and CaO (3.85-19.37 wt.%, average 8.84 wt.%) are the top three (Table 1). The contents of Fe_2O_3 (1.65-7.05 wt.%, average 5.07 wt.%), MgO (2.02-8.09 wt.%, average 4.75 wt.%), K_2O (1.10-4.83 wt.%, average 3.29 wt.%) are all more than 1%. The contents of Na_2O and FeO are around 1 wt.%, and the contents of TiO_2, MnO and P_2O_5 are all less than 1 wt.%. And the major element contents of all samples were allocated according to the Average Post-Archean Australian Shale (PAAS), almost all the contents of SiO_2, Al_2O_3, Fe_2O_3, TiO_2 and MnO in Well ZK0303 are lower than PAAS (Figure 3A). In contrast, the contents of all CaO and MgO and most of Na_2O were higher than those of PAAS and show strong enrichment (Figure 3A).

Table 1. Major elements from the samples of well ZK0303, Jiangling depression.

No.	Depth	SiO_2	Al_2O_3	Fe_2O_3	TiO_2	MnO	CaO	MgO	K_2O	Na_2O	P_2O_5	FeO	LOI
	m	wt%	wt%	wt%	wt%	wt%	wt%	wt%	wt%	wt%	wt%	wt%	wt%
ZK1	339	43.84	14.49	5.47	0.61	0.12	7.67	5.87	3.37	1.19	0.16	1.54	16.9
ZK2	363	58.40	10.13	3.79	0.51	0.07	8.10	2.77	2.36	1.93	0.12	1.45	11.4
ZK3	387	27.91	8.73	3.21	0.34	0.11	15.98	7.87	1.91	1.70	0.12	1.68	11.5
ZK4	400.5	52.83	11.96	4.28	0.64	0.11	8.45	3.97	2.55	2.31	0.11	0.90	12.3
ZK5	457	25.56	8.04	2.76	0.30	0.05	15.98	7.30	1.97	3.91	0.12	1.45	20.1
ZK6	504.5	15.65	4.14	1.65	0.17	0.03	11.85	8.09	1.12	14.44	0.06	0.84	16.7
ZK7	538.5	16.13	4.27	1.79	0.16	0.04	14.32	4.44	1.10	12.62	0.05	0.94	14.3
ZK8	550	43.88	13.52	5.17	0.61	0.08	6.34	4.53	3.42	3.82	0.13	1.78	16.6
ZK9	573	37.08	9.65	3.61	0.44	0.06	10.50	5.81	2.62	4.20	0.10	1.35	18.0
ZK10	585	28.37	8.89	3.37	0.36	0.06	13.38	4.72	2.29	6.30	0.11	1.20	15.2
ZK11	601	35.55	9.57	3.79	0.41	0.08	13.38	7.06	2.52	2.39	0.13	1.94	22.1
ZK12	620.5	26.33	7.25	2.80	0.31	0.07	15.29	8.03	1.68	4.75	0.10	1.29	22.5
ZK13	650	40.97	12.08	4.74	0.52	0.08	10.42	3.65	2.74	3.30	0.19	2.24	16.2
ZK14	681.5	55.94	11.79	4.34	0.61	0.08	8.76	2.02	2.87	1.99	0.10	1.60	11.0
ZK15	710	51.70	16.26	6.49	0.66	0.06	5.28	2.67	4.12	2.25	0.11	1.44	9.9
ZK16	779.5	49.33	16.76	6.30	0.61	0.05	4.87	3.60	4.83	1.82	0.15	2.51	11.1
ZK17	790	50.12	11.01	4.77	0.64	0.06	11.91	2.49	2.63	2.01	0.12	1.90	13.8
ZK18	809.9	22.91	6.29	2.18	0.26	0.08	19.37	7.74	1.23	1.61	0.10	1.90	10.7
ZK19	853	49.94	16.84	6.57	0.68	0.06	3.85	5.14	4.33	1.69	0.19	2.72	17.1
ZK20	870	43.87	14.42	5.55	0.58	0.05	8.57	4.49	3.68	1.44	0.14	1.61	10.6
ZK21	911.5	41.73	15.22	6.06	0.52	0.09	7.28	6.93	3.87	1.46	0.20	1.90	10.8
ZK22	930.5	45.32	16.36	6.86	0.58	0.05	5.55	5.51	4.40	1.29	0.17	2.22	9.6

Preprints (www.preprints.org) | NOT PEER-REVIEWED | Posted: 8 November 2023 doi:10.20944/preprints202311.0490.v1

ZK23	951	48.27	16.64	6.23	0.63	0.06	5.57	3.98	4.14	1.92	0.16	2.01	14.7
ZK24	970.5	40.03	13.35	5.30	0.50	0.06	10.50	5.55	3.38	1.09	0.14	2.26	13.3
ZK25	977.5	47.69	17.13	6.27	0.64	0.05	5.21	4.29	4.60	1.25	0.16	1.93	11.9
ZK26	993	45.97	15.97	6.25	0.56	0.04	5.13	6.15	4.12	1.32	0.17	2.20	12.7
ZK27	1027.5	51.74	10.46	3.87	0.60	0.08	9.25	4.22	2.33	1.44	0.13	1.56	12.8
ZK28	1040	48.54	16.68	6.83	0.67	0.06	5.17	4.50	4.32	1.08	0.15	2.02	14.9
ZK29	1050	45.90	15.57	6.03	0.56	0.05	6.31	4.97	4.05	0.97	0.16	2.02	12.0
ZK30	1090	47.59	17.58	6.82	0.62	0.06	4.43	5.65	4.34	1.09	0.18	2.19	12.0
ZK31	1099.5	48.27	17.07	6.44	0.63	0.07	4.78	4.94	4.36	1.08	0.17	1.91	11.2
ZK32	1129.5	51.33	12.46	4.66	0.63	0.06	9.67	3.43	3.00	1.21	0.12	1.52	13.0
ZK33	1145	48.35	17.61	6.95	0.64	0.05	4.51	3.98	4.74	0.99	0.16	2.28	11.5
ZK34	1175	47.81	14.60	6.07	0.65	0.07	8.79	3.95	3.76	1.04	0.15	1.74	12.6
ZK35	1185	48.63	16.42	6.21	0.63	0.07	6.40	4.35	4.20	1.10	0.15	1.70	11.3
ZK36	1203.5	42.85	14.59	4.87	0.56	0.10	8.87	6.60	3.43	1.00	0.15	2.04	16.5
ZK37	1213.5	46.39	16.34	5.71	0.66	0.09	5.77	6.76	3.80	1.21	0.18	2.26	13.1
ZK38	1260	50.10	14.15	5.75	0.66	0.06	7.89	3.96	3.39	1.18	0.16	1.84	12.2
ZK39	1295	40.04	13.50	4.96	0.52	0.06	10.47	3.98	3.31	0.90	0.13	1.57	11.1
ZK40	1325	39.47	9.79	3.08	0.52	0.06	13.90	2.96	2.28	0.98	0.10	1.44	11.3
ZK41	1346.5	48.45	16.38	6.19	0.60	0.08	4.57	6.40	3.94	1.05	0.16	2.11	11.8
ZK42	1370.5	52.52	11.72	4.64	0.63	0.11	9.54	3.20	2.55	1.64	0.14	1.59	12.9
ZK43	1388.5	47.69	13.29	5.39	0.65	0.07	9.42	4.48	3.17	0.96	0.15	1.98	13.5
ZK44	1426.5	36.28	12.75	4.57	0.46	0.07	16.50	4.34	3.16	1.27	0.15	2.45	17.9
ZK45	1434.5	49.47	16.79	7.01	0.66	0.05	4.84	4.34	4.53	0.86	0.17	2.25	10.7
ZK46	1457.5	50.46	15.80	5.60	0.71	0.05	6.79	3.66	4.04	0.96	0.15	1.89	11.7
ZK47	1465	51.78	16.31	6.58	0.66	0.07	4.91	3.92	4.05	1.17	0.15	1.94	10.3
ZK48	1485	54.15	13.76	5.00	0.63	0.09	6.85	3.37	3.23	1.31	0.14	1.72	10.9
ZK49	1505.5	38.27	11.79	4.63	0.48	0.11	16.44	3.31	2.86	1.00	0.11	2.08	14.2
ZK50	1525.5	51.27	9.04	3.54	0.57	0.11	11.15	4.27	1.94	1.17	0.12	1.78	14.5
ZK51	1543	46.84	16.56	5.87	0.61	0.07	5.86	5.28	4.41	0.94	0.18	2.60	12.0
ZK52	1560.5	49.50	17.71	7.05	0.65	0.05	3.44	4.86	4.54	0.96	0.15	3.49	9.1
ZK53	1567	50.03	11.60	4.91	0.65	0.06	11.30	3.19	2.88	1.09	0.14	1.74	13.9
ZK54	1581.5	47.64	14.62	5.24	0.60	0.08	7.49	4.31	3.70	1.04	0.15	2.00	13.1
ZK55	1599.5	55.45	12.25	4.70	0.61	0.06	7.22	3.64	3.01	1.25	0.14	1.88	11.6

Preprints (www.preprints.org) | NOT PEER-REVIEWED | Posted: 8 November 2023 doi:10.20944/preprints202311.0490.v1

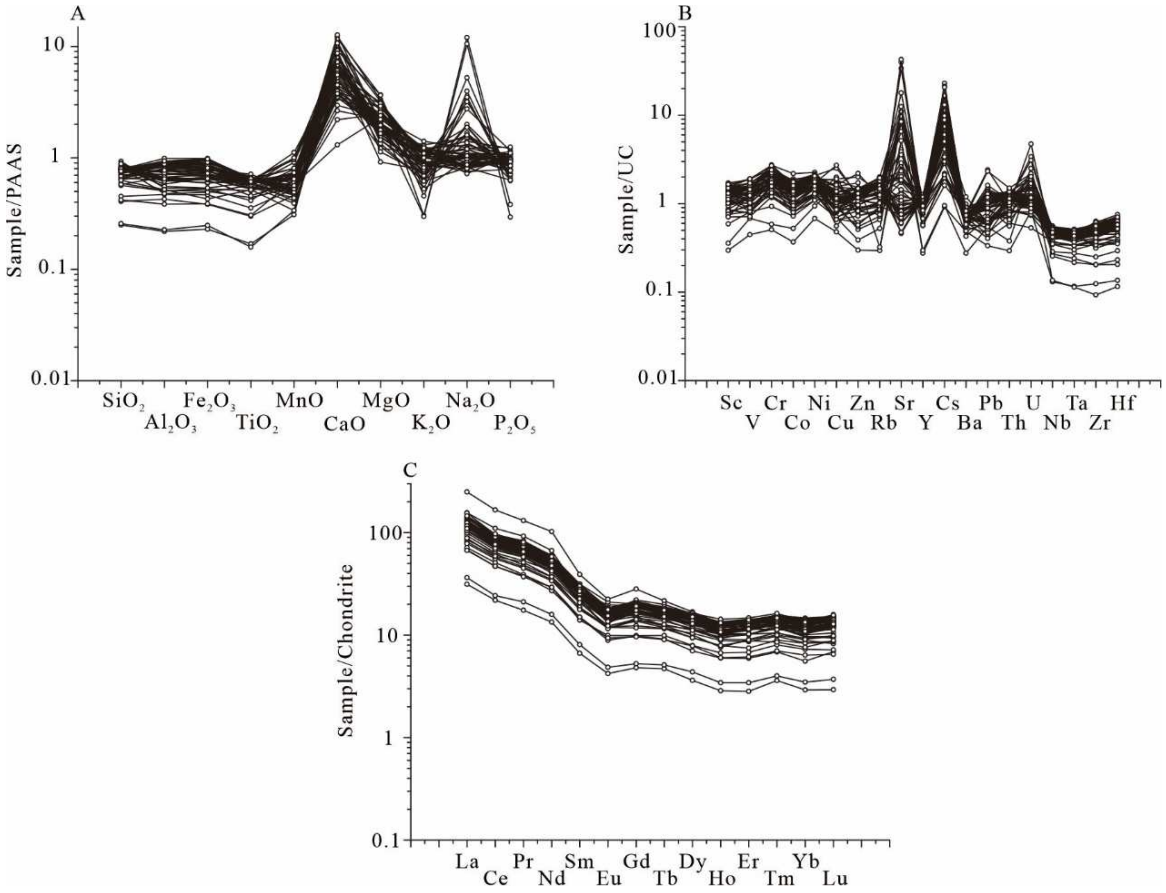

Figure 3. (A) PAAS-normalized major element diagram of samples in Well ZK0303, Data of the PAAS are from McLennan, 1989; (B) UC-normalized trace-element diagram of samples in Well ZK0303, Data of the UC are from Taylor & McLennan, 1985; (C) Chondrite-normalized rare element diagram of samples in Well ZK0303, Data of the Chondrite are from Boynton, 1984.

4.2. Trace and Rare Elements Geochemistry

The three elements with the highest average content are Sr (161.0-14887.0 ppm), Ba (152-656 ppm) and Rb (33.0-225.0 ppm), and their average contents are 2044.8 ppm, 383.9 ppm and 144.6 ppm, respectively (Table 2). And the contents of U (1.5-13.2 ppm, average 4.2 ppm), Hf (0.7-4.4 ppm, average 3.0 ppm) and Ta (0.3-1.1 ppm, average 0.9 ppm) are the lowest. The preservation state of each element varies greatly if they are normalized to Upper Crust (UC) data. The contents of Sr and Cs are enriched relative to UC, the contents of Nb, Ta, Zr and Hf show strong depletion (Figure 3B).

For REE, the Ce contents range from 17.5 to 88 ppm, averaging 62.51 ppm, the La contents range from 9.4 to 74.7 ppm, averaging 35.11 ppm, and the Nd contents range from 8.04 to 61.40 ppm, averaging 29.34 ppm (Table 3). They are the three most abundant REEs. The LREE/HREE ratios range from 7.70 to 13.83, averaging 8.93. In the chondrite-normalized diagram (Figure 3C), all samples show a set of steep dips of the light REE (LREE) curves, whilst the curves of the heavy REE (HREE) are flat. And Eu contents represent negative anomalies, they are V-shaped in the standardized diagram.

Preprints (www.preprints.org) | NOT PEER-REVIEWED | Posted: 8 November 2023 doi:10.20944/preprints202311.0490.v1

Table 2. Trace elements from the samples of well ZK0303, Jiangling depression.

No.	Depth	Sc	V	Cr	Co	Ni	Cu	Zn	Ga	Rb	Sr	Y	Cs	Ba	Pb	Th	U	Nb	Ta	Zr	Hf	B
	m	ppm	ppm	ppm	ppm	ppm	ppm	ppm	ppm	ppm	ppm	ppm	ppm	ppm	ppm	ppm	ppm	ppm	ppm	ppm	ppm	ppm
ZK1	339	14.3	90.7	75.9	15.7	36.8	36.0	83.7	18.8	141.0	1440.0	21.1	15.3	363.0	22.2	9.3	5.4	12.2	0.9	88.3	2.6	93.5
ZK2	363	9.4	47.0	54.8	8.0	24.4	49.7	51.6	12.6	93.0	498.0	18.3	8.0	344.0	6.1	6.5	1.5	9.3	0.7	75.7	2.2	62.4
ZK3	387	8.6	70.5	44.6	9.0	28.1	23.0	65.9	11.1	78.6	1033.0	13.8	7.0	276.0	17.4	6.9	5.6	7.1	0.5	51.7	1.7	75.8
ZK4	400.5	11.3	67.4	66.3	12.6	31.8	17.5	65.3	15.3	105.0	256.0	23.0	7.6	412.0	14.0	10.2	2.5	12.1	1.0	103.0	3.5	94.1
ZK5	457	7.9	75.6	40.8	8.6	25.8	24.5	36.3	10.4	73.5	1353.0	12.4	8.1	236.0	10.6	7.4	7.0	6.8	0.5	38.8	1.2	74.9
ZK6	504.5	3.3	26.7	17.8	3.7	13.6	12.0	21.2	4.2	33.0	3393.0	6.1	3.4	265.0	5.0	3.1	2.3	3.3	0.3	23.6	0.8	86.6
ZK7	538.5	3.9	40.9	20.4	5.2	18.8	39.0	122.0	5.3	36.0	1803.0	6.5	3.5	152.0	8.2	4.0	6.0	3.4	0.3	17.7	0.7	63.6
ZK8	550	13.9	87.8	64.5	13.8	30.3	43.1	61.6	18.1	117.0	834.0	21.7	10.5	390.0	18.4	14.2	5.9	13.5	1.1	59.6	2.2	180.0
ZK9	573	9.2	47.2	48.8	9.2	25.6	16.8	43.6	12.3	94.2	948.0	16.8	7.2	383.0	9.2	8.9	2.1	9.2	0.7	64.7	2.3	157.0
ZK10	585	8.6	58.8	42.9	8.8	24.6	22.5	38.9	11.1	81.0	3345.0	13.2	7.3	416.0	12.6	7.0	3.3	7.2	0.6	47.5	1.7	150.0
ZK11	601	9.5	70.8	52.3	10.3	29.5	32.5	40.5	13.1	105.0	3798.0	17.3	12.0	542.0	9.6	8.1	4.5	8.6	0.7	66.5	2.1	159.0
ZK12	620.5	6.5	48.5	32.5	7.2	21.8	17.4	27.5	8.4	58.6	3414.0	12.5	6.0	437.0	13.5	6.0	5.0	6.4	0.5	38.8	1.3	90.2
ZK13	650	12.6	92.3	62.4	13.3	33.1	34.7	56.2	16.4	112.0	609.0	19.4	11.1	298.0	21.8	12.1	9.5	11.2	0.9	64.6	2.0	130.0
ZK14	681.5	10.8	61.2	57.5	10.1	26.1	29.6	78.3	14.2	111.0	446.0	21.4	7.8	466.0	9.6	9.2	2.1	12.1	0.9	91.7	3.1	122.0
ZK15	710	15.1	96.7	74.5	14.5	35.7	13.9	77.8	21.0	147.0	209.0	24.1	12.5	480.0	14.2	13.4	2.4	13.0	1.0	113.0	4.0	194.0
ZK16	779.5	16.4	90.5	96.1	16.3	42.2	25.8	85.2	22.5	195.0	280.0	24.1	32.0	411.0	14.2	14.6	3.4	11.9	1.1	97.1	3.5	163.0
ZK17	790	10.4	69.1	60.0	9.4	29.6	21.7	60.6	13.4	113.0	339.0	22.2	17.8	270.0	9.4	11.6	3.3	12.7	1.1	87.3	3.2	93.3
ZK18	809.9	5.6	58.7	31.4	7.1	24.1	20.3	38.9	7.3	55.0	3208.0	9.1	10.4	303.0	28.3	6.6	13.1	5.3	0.4	35.6	1.4	51.4
ZK19	853	15.2	89.0	78.7	13.0	35.2	29.1	88.6	20.8	163.0	165.0	24.9	19.9	414.0	7.5	14.0	3.2	13.3	1.1	98.5	3.8	200.0
ZK20	870	13.1	82.8	65.9	10.2	31.3	19.8	68.3	17.8	138.0	1012.0	20.1	18.1	379.0	6.8	10.8	2.6	10.5	0.9	81.5	3.0	149.0
ZK21	911.5	15.9	96.8	78.9	14.9	38.3	46.2	107.0	21.3	173.0	3874.0	21.9	30.3	431.0	13.3	11.2	5.5	12.1	0.8	92.8	3.0	182.0
ZK22	930.5	17.0	90.4	83.6	16.9	41.5	62.7	89.5	21.8	186.0	692.0	24.3	24.7	472.0	17.1	14.0	3.9	12.6	1.0	94.4	3.3	207.0
ZK23	951	16.5	88.9	78.6	15.8	40.8	40.1	78.2	21.4	175.0	415.0	24.7	22.4	431.0	36.2	10.9	3.3	11.8	1.0	103.0	3.6	179.0

Preprints (www.preprints.org) | NOT PEER-REVIEWED | Posted: 8 November 2023 doi:10.20944/preprints202311.0490.v1

ZK24	970.5	13.4	79.4	72.6	15.0	38.6	29.9	78.2	17.2	168.0	1040.0	19.2	65.5	355.0	20.3	12.4	5.8	10.8	0.9	83.4	2.9	130.0
ZK25	977.5	17.8	114.0	94.8	21.9	45.0	31.0	96.0	22.6	203.0	303.0	23.9	30.8	499.0	17.0	14.7	3.0	14.0	1.0	96.7	3.5	198.0
ZK26	993	16.1	102.0	84.7	16.7	43.1	28.8	92.7	19.4	205.0	666.0	22.0	52.1	362.0	9.8	11.6	3.2	11.1	1.0	88.7	2.8	176.0
ZK27	1027.5	9.0	55.2	49.5	10.1	26.2	17.8	58.7	11.1	104.0	11837.0	19.2	31.1	399.0	9.1	8.7	2.3	10.8	0.8	84.7	2.6	84.7
ZK28	1040	16.7	103.0	86.7	18.2	42.9	26.4	98.9	21.6	204.0	272.0	25.8	39.5	361.0	14.3	13.1	2.8	13.1	1.0	100.0	3.5	137.0
ZK29	1050	16.5	95.2	85.6	13.8	40.6	20.3	97.7	21.2	204.0	639.0	22.8	50.2	370.0	8.9	12.4	2.6	11.2	0.9	82.8	3.1	138.0
ZK30	1090	16.9	114.0	86.3	15.4	39.5	34.5	107.0	21.6	198.0	1247.0	23.6	50.8	410.0	15.3	13.7	4.4	12.6	1.0	96.6	3.7	154.0
ZK31	1099.5	17.3	102.0	90.1	15.7	41.7	36.2	111.0	21.8	200.0	673.0	26.0	40.0	427.0	17.6	14.3	3.5	12.8	1.0	99.7	3.8	144.0
ZK32	1129.5	11.8	73.7	63.2	12.1	32.8	20.4	76.0	14.9	129.0	289.0	21.4	25.8	311.0	11.8	11.8	2.8	12.3	1.0	83.9	3.0	99.9
ZK33	1145	17.9	114.0	93.9	16.6	41.7	30.6	105.0	23.1	219.0	502.0	25.8	45.9	439.0	14.9	15.3	3.3	13.5	1.1	101.0	3.7	160.0
ZK34	1175	14.4	74.7	72.1	15.1	39.0	26.1	90.4	18.6	167.0	380.0	24.7	34.1	356.0	18.3	12.8	3.0	12.7	1.0	92.7	3.4	156.0
ZK35	1185	17.2	102.0	68.0	14.1	37.5	25.0	102.0	22.0	194.0	212.0	25.7	39.6	411.0	14.5	14.1	2.9	13.3	1.1	110.0	3.8	140.0
ZK36	1203.5	14.1	77.9	70.0	18.8	40.1	38.7	86.6	17.6	166.0	3076.0	22.2	58.6	406.0	20.7	11.8	4.5	10.9	0.9	88.6	3.3	45.0
ZK37	1213.5	15.0	85.2	70.6	14.6	36.6	29.5	89.9	18.2	167.0	6262.0	23.0	53.6	393.0	13.1	12.1	8.6	12.3	1.0	92.5	3.5	146.0
ZK38	1260	13.4	80.2	67.4	12.0	33.2	22.5	84.3	17.1	147.0	3030.0	23.0	34.6	414.0	16.2	12.7	3.2	12.4	1.1	89.4	3.4	125.0
ZK39	1295	13.2	75.3	62.3	15.1	36.3	24.5	80.9	16.9	155.0	3024.0	20.3	54.5	370.0	24.1	11.7	2.6	10.0	0.9	86.2	3.2	149.0
ZK40	1325	8.3	48.7	46.2	9.5	25.8	16.5	51.5	10.4	95.9	13868.0	14.9	25.1	656.0	9.1	8.5	3.8	9.3	0.8	72.1	2.5	105.0
ZK41	1346.5	16.3	74.0	54.3	13.6	34.6	25.9	93.3	20.1	189.0	708.0	24.5	50.5	450.0	9.3	12.5	4.7	12.0	1.0	102.0	3.9	138.0
ZK42	1370.5	11.7	69.5	55.8	12.2	29.2	20.8	75.9	14.4	114.0	323.0	25.8	22.3	357.0	16.3	11.5	2.8	13.1	1.1	102.0	4.0	103.0
ZK43	1388.5	13.0	68.8	65.6	19.0	39.0	28.1	83.1	15.6	144.0	2288.0	23.6	39.9	356.0	20.1	12.3	3.7	12.3	1.0	94.2	3.4	122.0
ZK44	1426.5	12.2	79.2	60.5	12.5	36.1	47.5	142.0	15.3	153.0	2804.0	18.8	84.6	363.0	13.8	10.3	13.2	8.8	0.7	70.4	2.5	96.9
ZK45	1434.5	17.4	61.6	77.9	16.4	41.1	25.8	101.0	21.2	216.0	161.0	26.0	61.9	389.0	14.5	15.0	3.4	13.4	1.1	99.5	3.6	147.0
ZK46	1457.5	15.9	60.4	58.7	13.1	36.9	21.1	89.0	19.1	202.0	816.0	26.0	61.8	366.0	10.0	14.5	3.0	13.8	1.1	111.0	4.1	113.0
ZK47	1465	16.2	72.9	64.5	13.8	34.8	25.6	89.4	20.4	178.0	165.0	27.9	42.2	456.0	13.3	13.0	3.4	13.3	1.1	116.0	4.4	116.0
ZK48	1485	13.2	87.5	66.5	18.2	34.1	67.9	85.2	17.1	140.0	647.0	26.1	31.9	403.0	17.7	11.9	3.3	13.0	1.0	108.0	3.8	99.4
ZK49	1505.5	12.0	58.9	58.5	16.5	44.4	25.8	66.7	14.4	144.0	857.0	19.1	56.1	268.0	43.5	10.7	4.6	9.7	0.8	75.6	2.9	83.2

Preprints (www.preprints.org) | NOT PEER-REVIEWED | Posted: 8 November 2023 doi:10.20944/preprints202311.0490.v1

ZK50	1525.5	7.8	42.8	42.0	8.0	21.8	28.3	58.6	9.1	84.1	14887.0	18.4	27.5	298.0	7.0	8.1	2.9	10.6	0.8	77.9	3.0	72.8
ZK51	1543	16.5	71.8	64.6	16.4	38.0	27.5	97.9	19.7	225.0	4382.0	24.6	78.5	411.0	19.2	14.6	5.3	12.7	1.0	96.3	3.7	115.0
ZK52	1560.5	18.2	86.8	84.1	17.6	41.0	38.2	105.0	22.5	218.0	242.0	26.0	76.3	406.0	34.9	16.0	6.1	13.1	1.1	106.0	4.1	141.0
ZK53	1567	11.1	61.2	58.3	11.4	33.4	40.6	156.0	12.8	132.0	287.0	23.8	27.6	306.0	15.3	11.7	2.7	12.7	1.0	94.6	3.4	92.4
ZK54	1581.5	14.4	74.3	60.7	15.9	35.4	29.8	92.6	16.3	165.0	2949.0	21.3	48.4	454.0	17.6	12.2	5.7	11.5	0.9	90.4	3.4	108.0
ZK55	1599.5	12.3	53.6	54.9	11.3	31.5	28.6	68.4	14.6	140.0	264.0	20.7	32.6	319.0	8.2	11.0	2.5	11.8	1.0	89.5	3.0	80.4

Preprints (www.preprints.org) | NOT PEER-REVIEWED | Posted: 8 November 2023 doi:10.20944/preprints202311.0490.v1

Table 3. Rare elements from the samples of well ZK0303, Jiangling depression.

No.	Depth	La	Ce	Pr	Nd	Sm	Eu	Gd	Tb	Dy	Ho	Er	Tm	Yb	Lu
	m	ppm	ppm	ppm	ppm	ppm	ppm	ppm	ppm	ppm	ppm	ppm	ppm	ppm	ppm
ZK1	339	33.8	61.9	7.1	27.1	4.9	1.0	4.4	0.7	4.2	0.7	2.2	0.4	2.1	0.3
ZK2	363	25.6	49.6	5.8	22.1	3.7	0.8	3.7	0.6	3.2	0.5	1.9	0.3	1.9	0.3
ZK3	387	23.1	44.4	5.3	18.3	3.2	0.6	3.0	0.5	2.7	0.4	1.6	0.2	1.4	0.2
ZK4	400.5	33.9	60.1	7.7	28.5	5.0	1.2	4.8	0.9	4.3	0.8	2.7	0.4	2.2	0.4
ZK5	457	20.4	37.5	4.5	16.3	3.0	0.6	2.6	0.5	2.2	0.4	1.3	0.2	1.2	0.2
ZK6	504.5	9.4	17.5	2.1	8.0	1.3	0.3	1.3	0.2	1.2	0.2	0.6	0.1	0.6	0.1
ZK7	538.5	10.9	19.4	2.5	9.5	1.6	0.3	1.4	0.3	1.4	0.2	0.7	0.1	0.7	0.1
ZK8	550	39.5	68.1	8.3	31.8	5.2	1.2	4.8	0.9	4.5	0.8	2.4	0.4	2.4	0.4
ZK9	573	24.4	46.1	5.6	21.0	3.7	0.8	3.2	0.6	3.3	0.6	1.8	0.3	1.8	0.3
ZK10	585	21.4	40.7	4.7	17.5	2.8	0.7	2.6	0.5	2.5	0.5	1.4	0.2	1.5	0.2
ZK11	601	23.4	44.5	5.4	20.3	3.6	0.8	3.1	0.6	3.0	0.6	1.6	0.3	1.8	0.3
ZK12	620.5	20.1	37.6	4.4	17.6	3.0	0.7	2.5	0.5	2.5	0.4	1.3	0.2	1.3	0.2
ZK13	650	33.8	59.2	7.2	27.1	4.5	1.1	4.0	0.7	3.6	0.7	2.1	0.4	2.0	0.3
ZK14	681.5	31.0	57.3	7.2	27.9	4.5	1.0	4.2	0.8	3.8	0.7	2.3	0.4	2.3	0.4
ZK15	710	35.0	65.0	7.9	32.4	5.4	1.3	4.8	0.9	4.8	0.9	2.9	0.5	3.1	0.5
ZK16	779.5	42.0	73.6	8.9	33.5	5.2	1.4	5.0	0.8	5.1	0.9	2.8	0.5	3.0	0.5
ZK17	790	33.3	59.5	7.5	29.9	5.0	1.2	4.5	0.8	4.5	0.8	2.5	0.4	2.6	0.4
ZK18	809.9	15.0	26.9	3.5	14.0	2.2	0.5	2.0	0.4	1.9	0.3	1.0	0.2	1.1	0.2
ZK19	853	39.4	70.2	8.7	35.2	6.3	1.5	5.2	0.9	5.3	0.9	2.9	0.5	3.0	0.5
ZK20	870	33.3	61.6	7.6	29.3	4.8	1.0	4.6	0.8	4.1	0.7	2.2	0.4	2.5	0.4
ZK21	911.5	46.9	88.0	11.1	40.0	5.2	1.1	5.2	0.8	4.1	0.8	2.5	0.4	2.2	0.4
ZK22	930.5	40.2	63.4	8.3	32.6	5.4	1.2	5.1	0.8	4.7	0.9	2.7	0.5	2.8	0.4
ZK23	951	35.6	64.1	8.1	31.0	5.1	1.0	4.8	0.9	4.6	0.9	2.7	0.4	2.7	0.5
ZK24	970.5	39.5	71.1	8.5	33.1	4.8	1.0	4.6	0.7	3.9	0.7	2.3	0.3	2.1	0.3
ZK25	977.5	74.7	133.0	15.7	61.4	7.8	1.6	7.3	1.1	5.4	0.9	3.0	0.5	2.7	0.4
ZK26	993	37.6	62.9	8.0	31.6	5.1	0.9	4.4	0.8	4.0	0.8	2.5	0.4	2.4	0.4
ZK27	1027.5	28.1	50.9	6.4	25.6	4.3	1.0	4.0	0.6	3.7	0.7	2.1	0.4	2.0	0.3
ZK28	1040	42.3	71.7	8.9	34.3	5.4	1.1	5.2	0.9	4.9	0.9	2.7	0.4	2.9	0.4
ZK29	1050	39.4	67.9	7.7	31.2	4.9	1.0	4.4	0.8	4.2	0.8	2.4	0.4	2.5	0.4
ZK30	1090	39.4	68.9	8.3	33.0	5.5	1.2	4.9	0.9	4.8	0.8	2.6	0.4	2.5	0.4
ZK31	1099.5	41.7	72.4	8.9	35.0	6.0	1.3	5.4	0.9	5.0	1.0	2.9	0.5	2.9	0.4
ZK32	1129.5	33.6	58.4	7.3	29.1	5.1	1.1	4.3	0.8	4.1	0.8	2.4	0.4	2.5	0.4
ZK33	1145	46.5	76.7	9.6	36.2	6.2	1.3	5.6	0.9	5.0	1.0	3.0	0.4	2.9	0.5
ZK34	1175	38.1	68.4	8.4	33.1	6.0	1.2	5.1	0.9	5.0	0.9	2.8	0.4	2.6	0.4
ZK35	1185	41.6	73.4	9.1	35.7	6.3	1.3	5.4	0.9	5.3	0.9	2.9	0.5	2.8	0.4
ZK36	1203.5	34.3	60.6	7.5	28.0	5.0	1.0	4.6	0.8	4.6	0.8	2.5	0.4	2.4	0.4
ZK37	1213.5	36.8	62.1	8.0	29.8	5.4	1.1	4.7	0.8	4.5	0.8	2.4	0.4	2.5	0.4
ZK38	1260	37.8	65.6	8.6	31.8	5.6	1.2	5.0	0.8	4.7	0.8	2.7	0.4	2.4	0.4
ZK39	1295	31.5	58.9	7.2	26.3	4.6	1.0	4.2	0.7	4.1	0.7	2.4	0.4	2.3	0.4
ZK40	1325	29.8	53.9	6.9	24.1	4.3	0.8	3.6	0.6	3.0	0.6	1.9	0.3	1.6	0.3
ZK41	1346.5	35.9	66.0	8.4	29.0	5.6	1.2	4.9	0.8	4.6	0.9	2.7	0.5	2.8	0.4
ZK42	1370.5	41.3	76.2	10.0	35.6	6.0	1.2	5.7	1.0	5.2	0.9	2.9	0.4	2.7	0.4
ZK43	1388.5	36.0	64.5	8.6	30.6	5.3	1.2	5.0	0.8	4.7	0.8	2.8	0.4	2.4	0.4
ZK44	1426.5	31.3	56.2	7.0	25.3	4.5	0.8	3.8	0.7	3.7	0.7	2.2	0.3	2.0	0.3
ZK45	1434.5	43.1	74.2	9.6	34.1	6.0	1.2	5.3	0.9	5.0	0.9	2.9	0.4	2.5	0.4
ZK46	1457.5	41.8	73.5	9.5	33.3	6.0	1.2	5.3	0.9	4.9	0.9	3.0	0.4	2.6	0.4
ZK47	1465	38.4	67.2	8.9	32.1	6.1	1.3	5.4	1.0	5.2	1.0	3.1	0.5	2.8	0.5
ZK48	1485	35.4	62.5	7.9	29.5	5.7	1.1	4.8	0.8	4.9	0.9	2.9	0.4	2.7	0.4
ZK49	1505.5	29.9	58.3	6.9	25.8	4.6	0.8	3.8	0.7	3.8	0.7	2.2	0.3	1.9	0.3

 doi:10.20944/preprints202311.0490.v1

ZK501	525.5	26.5	47.0	6.2	22.2	4.1	0.9	3.7	0.6	3.6	0.6	1.9	0.3	1.9	0.3
ZK51	1543	41.7	70.5	8.8	31.8	5.9	1.3	5.0	0.9	4.8	0.9	2.7	0.4	2.7	0.4
ZK521	560.5	42.4	72.7	9.3	35.1	6.0	1.1	5.1	0.9	4.9	0.9	2.9	0.4	2.8	0.5
ZK53	1567	34.8	63.3	7.9	29.5	5.6	1.2	4.8	0.9	4.8	0.8	2.6	0.4	2.5	0.4
ZK541	581.5	43.6	77.6	9.7	35.0	5.6	1.1	5.0	0.8	4.4	0.8	2.5	0.4	2.4	0.4
ZK551	599.5	32.9	61.3	7.8	28.5	5.4	1.1	4.5	0.8	4.1	0.8	2.4	0.3	2.3	0.3

5. Discussion

5.1. Palaeoclimate and Palaeoweathering

The elemental geochemistry, such as FeO/MnO, Al_2O_3/MgO, is a good indicator of palaeoclimate changes. This is because Mn content is relatively high in arid environment, while the opposite is true in humid environment. And Fe is easy to precipitate quickly in the form of Fe(OH) colloid in humid environments. So the high ratio of FeO/MnO in the sediment corresponds to the humid climate, while the low value is a response to the arid climate (Zhang et al., 2016). For Al_2O_3/MgO, the high value is a representative of water desalination and humid climate, while the low value indicates an arid climate. Worash (2002) believes that the distribution, composition and relative concentration of some trace elements in mudstone may indicate the palaeoclimate and palaeoenvironment. Zhao et al. (2007) and Cao et al. (2012) proposed using C-value as an indicator of palaeoclimate. The calculation formula of C-value is as follows: C-value = Σ(Fe + Mn + Cr + V + Ni + Co)/Σ(Ca + Mg + Sr + Ba + K + Na). This is because the Fe, Mn, Cr, V, Ni and Co elements are relatively enrich in humid conditions, while in arid conditions, evaporation precipitates saline minerals, resulting in the concentration of Ca, Mg, K, Na, Sr and Ba elements.

In arid climate, the source rocks are dominated by physical weathering, in which they can only be mechanically broken down into smaller grain sizes without significant changes in mineralogical and chemical composition (Wanas and Assal, 2020). And the chemical weathering plays a dominant role in humid climates and strongly controls the major and trace element composition of siliceous clastic sediments (Nesbitt and Young, 1982; Harnois, 1988; Middelburg et al., 1988; McLennan et al., 1993; Fedo et al., 1995). It directly affects the removal of mobile elements (Na, K, Ca) and the enrichment of immobile elements (Al, Si) in the sediments (Nesbitt and Young, 1982). The chemical index of alteration (CIA= $Al_2O_3/(Al_2O_3 + CaO^* + Na_2O + K_2O) \times 100$, Nesbitt and Young[13]; $CaO^* = CaO - 10/3 \times P_2O_5$, McLennan et al., 1993) can determine the mobility of elements during chemical weathering and potassium metasomatism during diagenesis, and evaluate the weathering history and source rock composition. Besides, chemical index of weathering (CIW= $Al_2O_3/(Al_2O_3 + CaO + Na_2O) \times 100$, Harnois, 1988), plagioclase index of alteration (PIA= $100\times (Al_2O_3 - K_2O)/(Al_2O_3 + CaO^* + Na_2O - K_2O)$, Fedo et al., 1995) are also important bases for assessing the source area-palaeoweathering. The higher the values of CIA, CIW and PIA indicate the stronger the chemical weathering in the source area (Nesbitt and Young, 1982).

In the Figure 4 and Table 4, the ratios of FeO/MnO, Al_2O_3/MgO and C-value have similar changing trends. From 1599.5 to 800 m, the ratio of FeO/MnO (from 15.00 to 64.63), Al_2O_3/MgO (from 0.81 to 4.42) and C-value (from 0.07 to 0.51) fluctuates in a large range, and the change frequency is high. The complex variation trends of FeO/MnO, Al_2O_3/MgO and C-value indicate that the climate in the Jiangling depression during the early-middle Paleocene was very unstable and changed rapidly between aridity and humidity, so the climate type should be semi-humid and semi-arid. The change of climate also changes the degree of chemical weathering in the source area. The ratios of CIA, CIW and PIA are well matched with the changes of climate indicators, such as Al_2O_3/MgO and C-value (Figure 4), indicating that the climate of alternating aridity and humidity during the early-middle Paleocene in the Jiangling depression greatly affected the degree of weathering in the source area. From 800 to 630 m, the ratios of FeO/MnO, Al_2O_3/MgO and C-value are higher, and the values of CIA, CIW and PIA are also increased (Figure 4). The simultaneous increased indicators of climate and chemical weathering show that during the late Paleocene to early Eocene, precipitation increased and the climate became humid, which led to the intensification of chemical weathering. From 630 to 339

Preprints (www.preprints.org) | NOT PEER-REVIEWED | Posted: 8 November 2023 doi:10.20944/preprints202311.0490.v1

m, the change trends of Al_2O_3/MgO, C-value and chemical weathering indicators (CIA, CIW and PIA) are different with FeO/MnO, they have several increases (Figure 4). This indicates that although the climate of the Eocene was generally arid, it became humidity in several times. And although the climate of Eocene was arid enough to allow the deposition of halite, it experienced a short-time humidity (Figure 4).

Table 4. Selected element ratios from samples of well ZK0303, Jiangling depression.

No.	FeO/MnO	Al_2O_3/MgO	C-value	CIA	CIW	PIA	U/Th	Ni/Co	V/Cr	Sr/Ba
ZK1	12.52	2.47	0.31	55.33	63.50	57.17	0.58	2.34	1.19	3.97
ZK2	20.14	3.66	0.25	45.77	51.23	44.62	0.23	3.06	0.86	1.45
ZK3	15.56	1.11	0.12	31.28	33.57	28.31	0.81	3.13	1.58	3.74
ZK4	8.26	3.01	0.25	48.03	53.51	47.53	0.24	2.52	1.02	0.62
ZK5	28.43	1.10	0.10	27.26	29.21	23.75	0.95	2.99	1.85	5.73
ZK6	24.71	0.51	0.05	13.21	13.70	10.38	0.73	3.69	1.50	12.80
ZK7	25.41	0.96	0.06	13.28	13.75	10.58	1.48	3.59	2.00	11.86
ZK8	23.12	2.98	0.29	50.67	58.12	50.90	0.42	2.20	1.36	2.14
ZK9	22.50	1.66	0.16	36.23	40.18	32.86	0.23	2.78	0.97	2.48
ZK10	20.69	1.88	0.13	29.14	31.25	25.46	0.47	2.78	1.37	8.04
ZK11	23.66	1.36	0.15	34.91	38.44	31.51	0.56	2.86	1.35	7.01
ZK12	18.43	0.90	0.10	25.32	26.90	22.04	0.84	3.02	1.49	7.81
ZK13	29.47	3.31	0.24	43.26	47.97	41.62	0.79	2.49	1.48	2.04
ZK14	20.78	5.84	0.28	47.02	53.10	46.14	0.23	2.58	1.06	0.96
ZK15	25.71	6.09	0.46	59.06	69.46	62.93	0.18	2.46	1.30	0.44
ZK16	55.78	4.66	0.42	60.32	73.01	65.82	0.23	2.59	0.94	0.68
ZK17	34.55	4.42	0.25	40.54	44.89	38.27	0.28	3.14	1.15	1.26
ZK18	23.75	0.81	0.07	22.34	23.61	19.69	1.99	3.4	1.87	10.59
ZK19	46.90	3.28	0.44	64.61	77.49	71.88	0.23	2.71	1.13	0.40
ZK20	31.57	3.21	0.31	52.16	60.18	52.95	0.24	3.07	1.26	2.67
ZK21	21.84	2.20	0.31	56.03	65.34	58.44	0.49	2.57	1.23	8.99
ZK22	41.89	2.97	0.41	60.54	72.32	65.63	0.28	2.46	1.08	1.47
ZK23	36.55	4.18	0.40	59.99	70.51	64.23	0.31	2.58	1.13	0.96
ZK24	37.05	2.41	0.26	47.92	54.73	47.25	0.47	2.57	1.09	2.93
ZK25	37.12	3.99	0.41	61.90	74.24	67.83	0.21	2.05	1.20	0.61
ZK26	51.16	2.60	0.38	61.51	73.11	66.86	0.28	2.58	1.20	1.84
ZK27	19.75	2.48	0.21	45.41	50.52	44.24	0.26	2.59	1.12	29.67
ZK28	35.44	3.71	0.46	62.38	74.06	68.29	0.21	2.36	1.19	0.75
ZK29	42.08	3.13	0.37	59.04	69.75	63.04	0.21	2.94	1.11	1.73
ZK30	39.11	3.11	0.44	65.46	78.08	72.84	0.32	2.56	1.32	3.04
ZK31	28.09	3.46	0.43	63.87	76.32	70.59	0.25	2.66	1.13	1.58
ZK32	26.21	3.63	0.27	48.06	54.73	47.47	0.23	2.71	1.17	0.93
ZK33	42.22	4.42	0.49	64.50	78.05	72.22	0.22	2.51	1.21	1.14
ZK34	24.17	3.70	0.35	52.70	60.98	53.71	0.23	2.58	1.04	1.07
ZK35	23.61	3.77	0.39	59.44	70.10	63.57	0.21	2.66	1.50	0.52
ZK36	20.40	2.21	0.25	53.24	60.86	54.32	0.38	2.13	1.11	7.58
ZK37	25.68	2.42	0.32	61.63	71.94	66.30	0.71	2.51	1.21	15.93
ZK38	29.68	3.57	0.35	54.25	62.35	55.74	0.25	2.77	1.19	7.32
ZK39	26.17	3.39	0.27	48.62	55.21	48.19	0.23	2.4	1.21	8.17
ZK40	23.23	3.31	0.15	36.79	40.23	34.05	0.44	2.72	1.05	21.14
ZK41	26.05	2.56	0.39	64.44	76.70	70.92	0.38	2.54	1.36	1.57
ZK42	15.00	3.66	0.28	46.88	52.14	46.08	0.24	2.39	1.25	0.90
ZK43	28.70	2.97	0.30	50.45	57.35	50.59	0.30	2.06	1.05	6.43
ZK44	36.03	2.94	0.18	38.44	42.49	35.72	1.28	2.89	1.31	7.72

Preprints (www.preprints.org) | NOT PEER-REVIEWED | Posted: 8 November 2023 doi:10.20944/preprints202311.0490.v1

ZK45	41.67	3.87	0.48	63.4876.6070.50	0.23	2.51	0.79	0.41
ZK46	35.00	4.32	0.36	58.3568.5861.90	0.21	2.82	1.03	2.23
ZK47	29.39	4.16	0.47	62.9174.5568.77	0.26	2.52	1.13	0.36
ZK48	19.33	4.08	0.34	55.7864.1857.83	0.27	1.87	1.32	1.61
ZK49	19.62	3.56	0.20	37.1640.8434.33	0.43	2.69	1.01	3.20
ZK50	16.18	2.12	0.18	39.4943.1537.35	0.36	2.74	1.02	49.96
ZK51	36.62	3.14	0.35	60.9272.7266.17	0.36	2.32	1.11	10.66
ZK52	64.63	3.64	0.51	67.7581.9977.20	0.38	2.33	1.03	0.60
ZK53	30.00	3.64	0.27	43.9349.3142.24	0.23	2.93	1.05	0.94
ZK54	24.69	3.39	0.32	55.4764.5357.61	0.46	2.23	1.22	6.50
ZK55	30.32	3.37	0.31	52.6360.4453.55	0.22	2.79	0.98	0.83

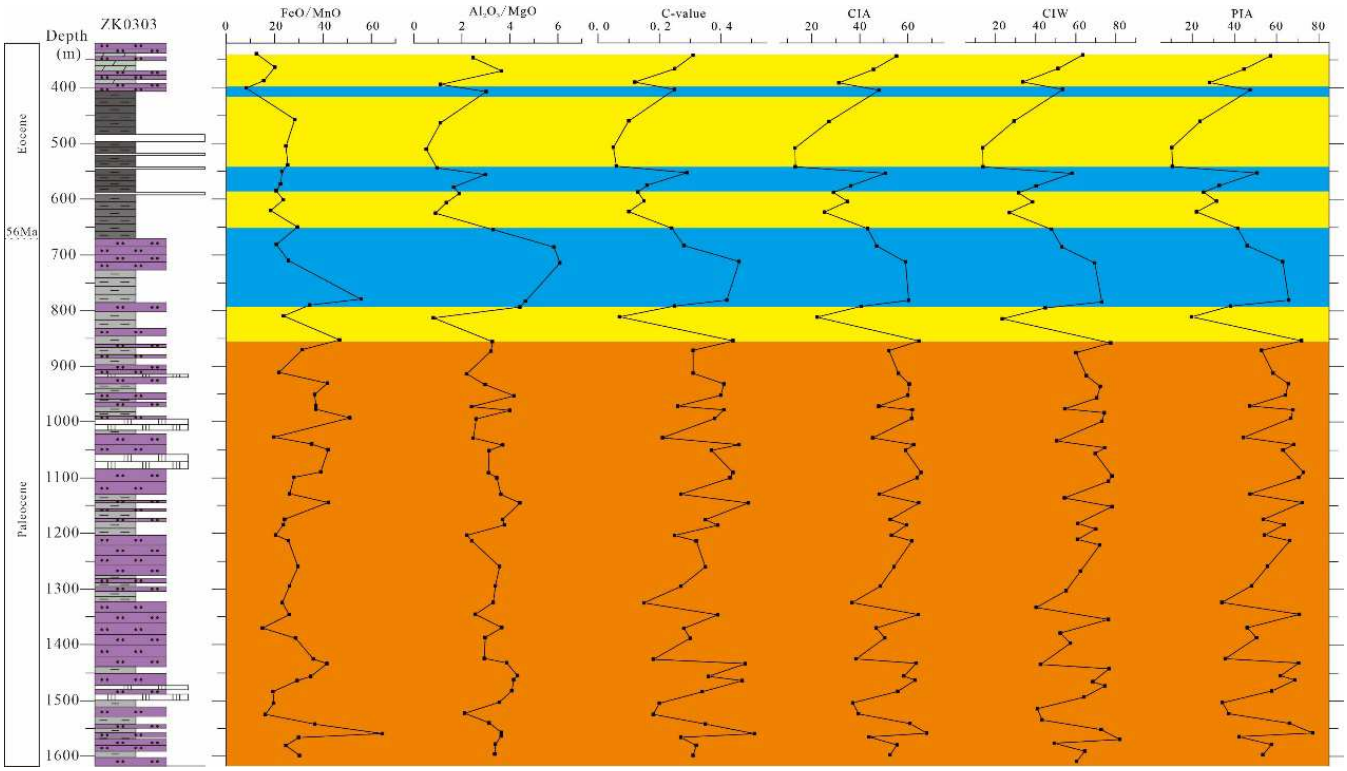

Figure 4. Distribution diagram of major and trace element ratios from well ZK0303, Jiangling depression (Legend as in Figure 2). Orange areas represent semi-humid to semi-arid environments, yellow areas represent arid environments, and blue areas represent humid environments.

The cause of the semi-humid to semi-arid climate of the Paleocene in Jianghan Basin may be related to the instability of the subtropical highs controlled by the planetary wind system (Lu et al., 2007; Johanson and Fu, 2009; Hasegawa et al., 2012). And this significant climate changes during the late Paleocene to early Eocene appears to be potentially linked to PETM (Paleocene-Eocene thermal maximum). During the PETM, the global water cycle changed, which also led to an increase in precipitation in the Jianghan Basin (Teng et al., 2021; Xie et al., 2022). On the one hand, the arid climate and the frequent short-time humidity of Eocene may be related to the instability of the subtropical highs, on the other hand, they may be related to the hyperthermals after the PETM, such as ETM2, H2, I1, I2 (Samanta et al., 2013; Chen et al., 2014; Abels et al., 2015).

5.2. Redox Conditions

The solubility of trace elements such as U, Ni, V, Mo, and Co is controlled by the redox conditions, so they are generally enriched in sediments formed in reducing environment[79-82](Francois, 1988; Authur and Sageman, 1994; Yuri et al., 2008; Hetzel et al., 2011). In the sedimentary environment, they are easily soluble under oxic condition, insoluble under anoxic condition, and

 doi:10.20944/preprints202311.0490.v1

almost no migration in diagenesis, maintaining the original record of deposition, so they can be used as a judge index to restore the redox environment of the ancient water (Tribovillard et al., 2006). In the study of late Jurassic redox environment in northwestern Europe, Jones and Manning (1994) concluded that the ratios of U/Th, Ni/Co, V/Cr are reliable substitutes for redox conditions. In general, the high ratios of U/Th, Ni/Co, V/Cr indicates a anoxic environment, while the low ratios indicates an oxic environment.

In the Figure 5 and Table 4, the values of U/Th, Ni/Co and V/Cr in the section of 1599.5 to 800 m are generally low, while the values in individual sediments are high. And in the 809.9 m, the ratios of U/Th, Ni/Co and V/Cr all showed an abnormal increase, but the indicators of climate and chemical weathering declined significantly (Figure 4). From 800 to 339 m, the range of low ratios of U/Th, Ni/Co and V/Cr almost coincide with the humid region, while the higher ratios of U/Th, Ni/Co and V/Cr are mostly in the arid region (Figure 5). According to the changes trends of U/Th, Ni/Co and V/Cr from 800 to 339 m, in the Eocene, the water body of lake in humid climate is in oxidation condition, while the water body of lake in arid climate is in reduction condition. The reason for this phenomenon may be that the lake is more likely to accept the replenishment of external water bodies in a humid environment, which makes the lake water rich in oxygen and the stratification is not strong, so the sediment at the bottom of the lake is mostly in oxidation condition. However, when the climate becomes arid, the external recharge is decreased, the lake is in a still water environment, the water body is obviously stratified, and the bottom of the lake is anoxic, making the sediment mostly in reduced condition. The rapid changes of arid and humid climate in the Paleocene allowed the lake to receive frequent replenishment from external water bodies, so that the sediments were almost in oxidation condition, except for extremely arid climates (such as a significant aridity recorded at 809.9 m).

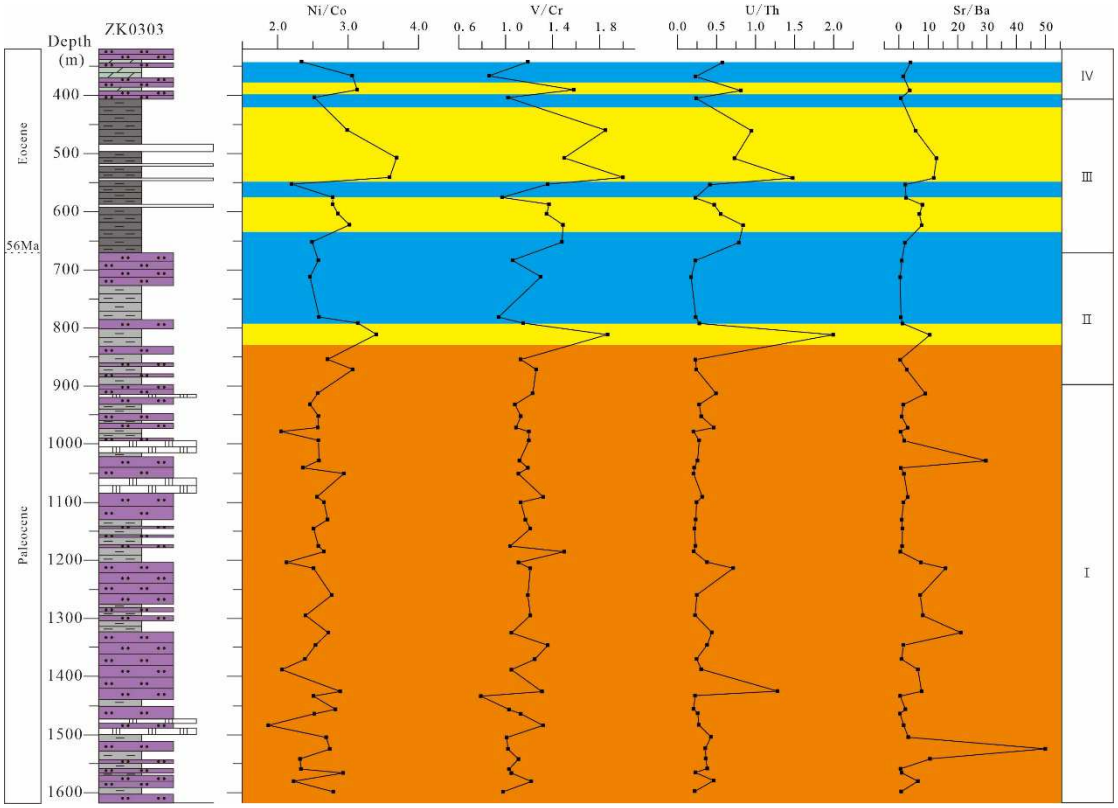

Figure 5. Distribution diagram of trace element ratios from well ZK0303, Jiangling depression (Legend as in Figure 2). Orange areas represent semi-humid to semi-arid environments, yellow areas represent arid environments, and blue areas represent humid environments. Stage I: playa-lake, stage II: brackish lake, stage III: saline lake, stage IV: brackish playa-lake.

5.3. Palaeosalinty

Preprints (www.preprints.org) | NOT PEER-REVIEWED | Posted: 8 November 2023 doi:10.20944/preprints202311.0490.v1

The most direct and effective way to distinguish lake salinity is to identify sedimentary sequences, especially in salt lake sedimentary systems. According to lithology, grain size and sedimentary structure, the 1600-320 m section of well ZK0303 is divided into four main lake facies types: playa lake, shallow to semi-deep brackish lake and deep saline lake and brackish playa lake (Figures 6 and 7).

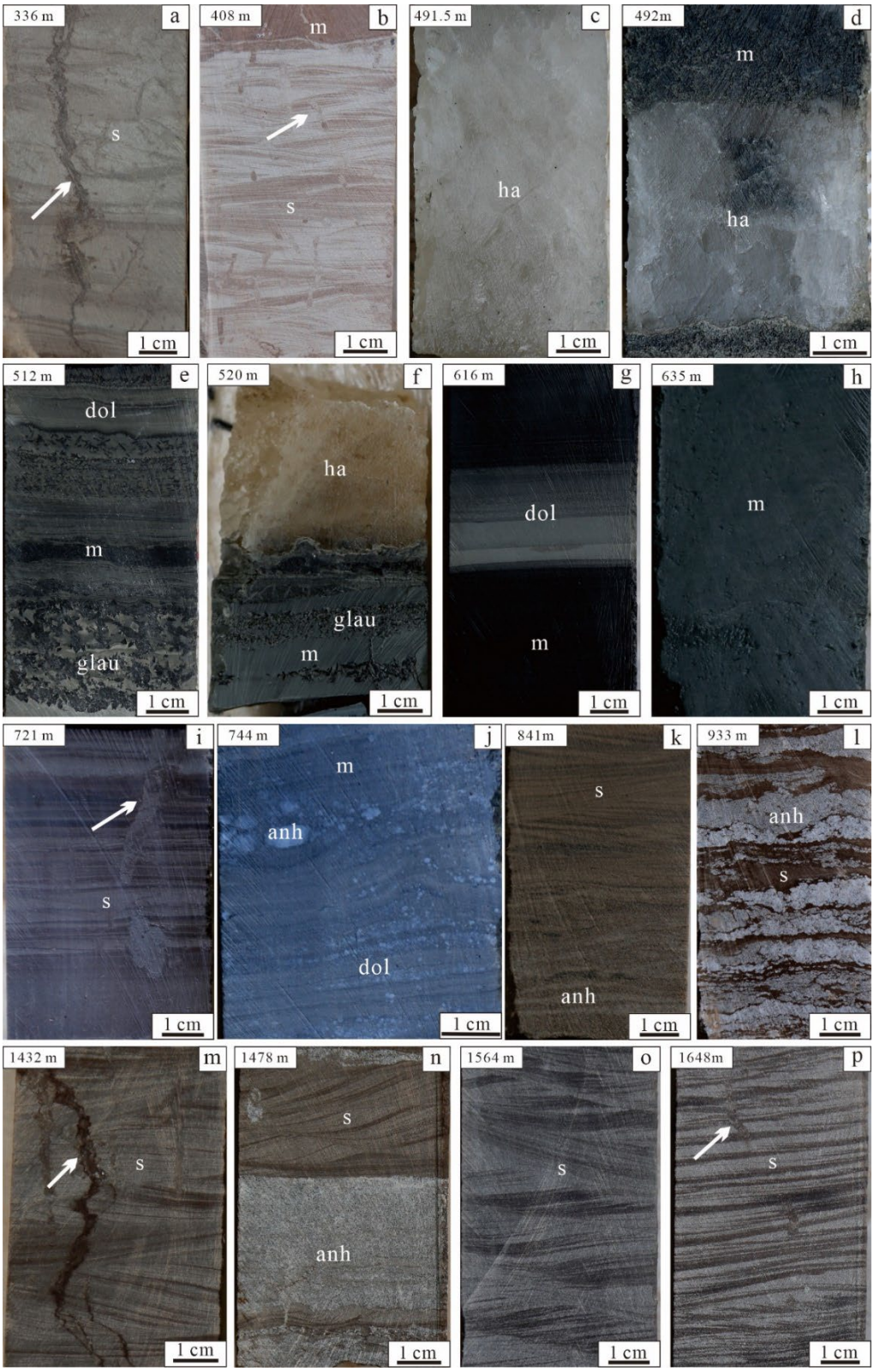

Figure 6. Photographs of major sedimentary structures in the 320-1600-m segment of well ZK0303. a: mud crack (white arrow); b: wavy cross-bedded siltstone, burrow (white arrow); c: massive halite; d:

Preprints (www.preprints.org) | NOT PEER-REVIEWED | Posted: 8 November 2023 doi:10.20944/preprints202311.0490.v1

conformable contact of halite and organic matter-rich mudstone*; e: mudstone interbedded with dolomite and glauberite; f: conformable contact of halite, glauberite and mudstone*; g: organic matter-rich mudstone interbedded with layered dolomite; h: massive mudstone*; i: cross-bedded siltstone, burrow (white arrow); j: thin-layer dolomite and banded anhydrite; k: cross-bedded siltstone and thin-layer anhydrite; l: siltstone interbedded with anhydrite; m: cross-bedded siltstone and mud crack (white arrow); n: herringbone cross-bedded and bedded anhydrite; o: herringbone cross-bedded siltstone; p: parallel-bedded siltstone, burrow (white arrow). All photographs are oriented vertically. m: mudstone; s: siltstone; ha: halite; dol: dolomite; glau: glauberite; anh: anhydrite. *potential hydrocarbon source rocks.

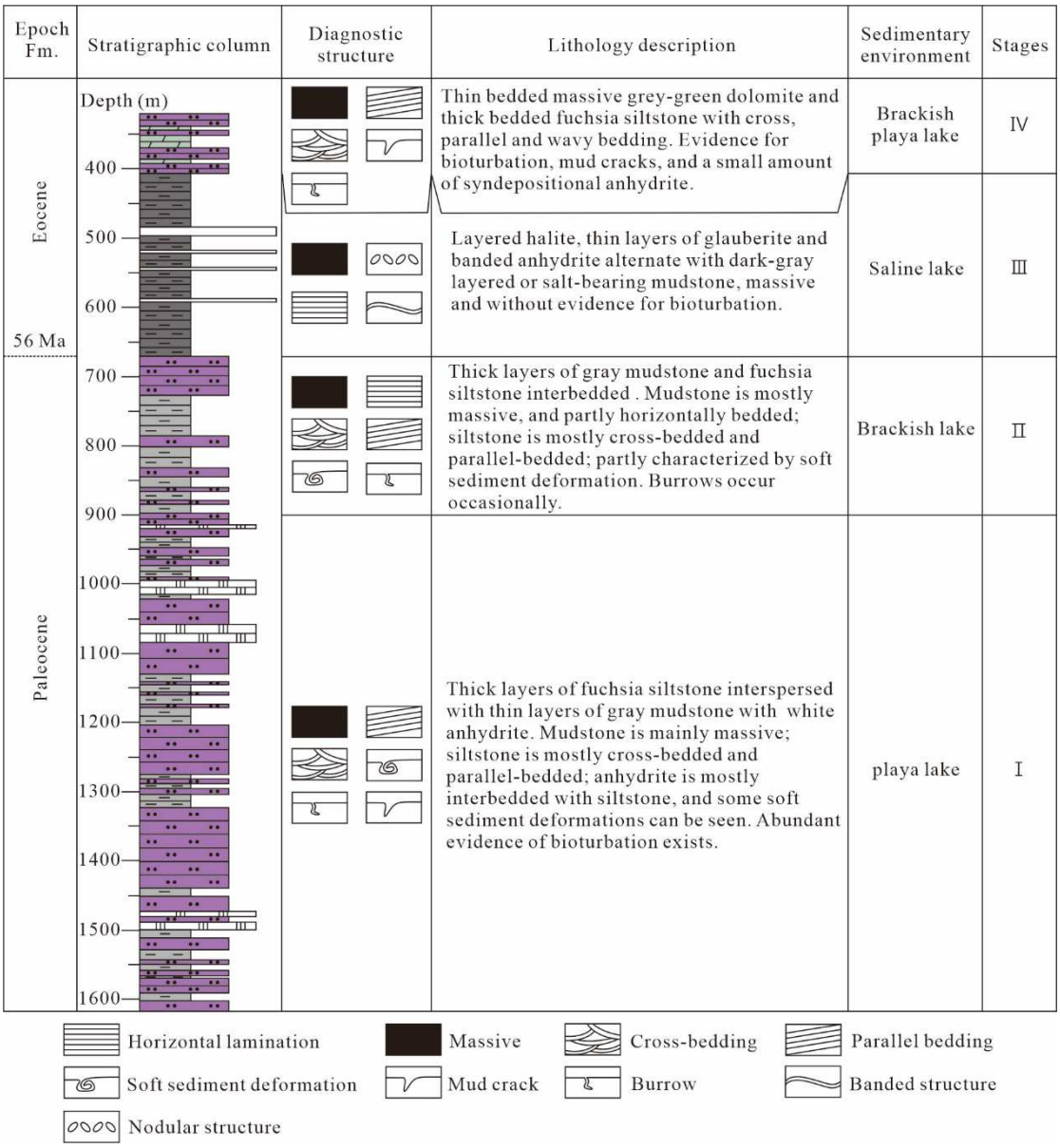

Figure 7. Lithofacies in the 320 to 1600 m section of well ZK0303 (Legend as in Figure 2).

Playa-lake (stage I):

Rocks are mainly composed of thick layers of mostly coarse-grained fuchsia-red siltstone, partly interbedded with grey mudstone and bedded white anhydrite (Figures 6 and 7). Bioturbation traces such as burrows and signs of exposure such as mud cracks occur in this section (Figures 6 m, n and p). And there are cross bedding, herringbone cross bedding and parallel bedding in the siltstones (Figures 6 n, o and p). The mostly relatively coarse grain size and the cross bedding indicate flowing

 doi:10.20944/preprints202311.0490.v1

waters, and the burrows and mud cracks show that the sediments were accumulated in shallow, well oxygenated waters and were exposed from time to time.

Brackish lake (stage II):

Mudstone and siltstone units are interbedded, and thin layers of anhydrite appear sporadically. (Figures 6 and 7). In this section, mud cracks formed in the exposed environment were not observed, and only a few bioturbation traces appeared (Figure 6 i). And siltstone and mudstone are mainly massive, and some sandstones are cross or parallel bedded (Figures 6 i and 1), while a small amount of mudstone are horizontally bedded (Figure 6 j). Horizontal bedded and bioturbation traces indicate a relatively calm semi-deep lake environment, while coarse-grained siltstone interbedded with fine-grained mudstone and cross bedding indicate a shallow lake environment and a dynamic hydrological environment with flow.

Saline lake (stage III):

This section is dominated by fine-grained dark gray mudstone, containing dolomite, anhydrite, glauberite, and halite (Figures 6 and 7). The mudstones are mostly massive (Figure 6 h), and they are partly horizontally bedded, or interbedded with banded anhydrites, thin layers of glauberite or halite (Figures 6 e and g). And in this section, the evidences for bioturbation or mud cracks were not observed. The horizontal bedding results from sediment accumulation in a stable calm environment.

Brackish playa-lake (stage IV):

Characteristics similar to those in the section between 1600-1200 m occur in the uppermost sequence of the core again, indicating the reestablishment of a playa-lake environment (Figures 6 and 7). However, in addition to siltstone, it is mainly dolomite, and anhydrite clumps are occasionally seen.

The climate of Jiangling depression was in rapid alternations of arid and humid during the early and middle Paleocene (Figure 5). In an arid climate, evaporation increases the salinity of the lake, and gypsum deposited, but when the climate becomes humidity, the salinity of the lake decreased due to weaker evaporation and increased recharge. Therefore, the salinity of lake water varied greatly in the early to middle Paleocene (stage I). The late Paleocene climate changed from an ephemeral extreme arid to a long-time humid (Figure 5), so the salinity of the lake water decreased (stage II). In the Eocene, the climate of Jiangling depression was mainly arid (Figure 5), the salinity of the lake increased and the halite deposited (stage III). Finally, as the climate changed to humid, the salinity of lake became less (stage IV).

Some trace elements are very sensitive to changes in salinity, so they can be used to indicate the paleosalinity, such as Sr/Ba ratio (Meng et al., 2012; Jia et al., 2013; Fu et al., 2016). In general, with the increase of salinity, Sr and Ba are precipitated by the formation of sulfate, but $BaSO_4$ preferentially precipitates, and $SrSO_4$ will precipitates when the salinity reaches a certain high value. Therefore, a high Sr/Ba ratio indicates a higher salinity of the water. From the Figure 5 and Table 4, in the stage I, the Sr/Ba ratio experienced multiple increases, indicating great changes in salinity. After that, the Sr/Ba ratio decreased and increased only in the significant arid (stage II). In stage III, Sr/Ba ratio increased, but decreased in humid region. In stage IV, the Sr/Ba ratio in humid region was lower than that in arid region.

The sedimentary sequences and Sr/Ba ratio show that the climate of Jiangling depression greatly controlled the salinity of lake water during the Paleocene to Eocene. The climate in the early and middle Paleocene alternated frequently between aridity and humidity, and the salinity of the lake varied greatly. During the late Paleocene-early Eocene, the climate changed from arid to humid, and the salinity of the lake water also changed from increasing to decreasing. In the Eocene, the climate was mainly arid, and the salinity of the lake increased, but when the humid climate came, the salinity of the lake would decrease again.

6. Conclusions

According to the chemical characteristics of major and trace elements, we reconstructed the environment of the Paleocene-Eocene saline lake in the Jiangling depression, southwestern Jianghan Basin, and obtained the following understandings:

(1) The Jiangling depression experienced a semi-humid to semi-arid climate during the early-middle Paleocene. There was a rapid shift to humid climate during the late Paleocene to early Eocene, following a short-time intense dryness. In the Eocene, the climate was arid, but it experienced many short humidity. The trend of chemical weathering is similar to that of climate change. The instability of the subtropical highs controlled by the planetary wind system, the hyperthermals (such as PETM, ETM2, H2, I1, I2) may be important factors in the climate changes.

(2) The climate of the Jiangling depression underwent frequent fluctuations between humid and arid conditions during the Paleocene-Eocene. In the humidity and alternations of aridity and humidity, the lake water received external water, resulting in a weak stratification of the lake water, so sediments are formed under the oxidation condition. In the aridity, the lake becomes a still water environment, which makes the sediment are formed under the reduced condition.

(3) Under the control of climatic condition, the salinity of the lake changed greatly in the early-middle Paleocene; from the late Paleocene to the early Eocene, the overall salinity of the lake was low; in the Eocene, the salinity of the lake increased, but there were still several decreases.

Author Contributions: K.Y. and C.L.W. designed the research and prepared the original manuscript. J.Y.W, R.Y.C. and L.H.L. revised the manuscript. R.Q.L. participated in sample collection and processing. All authors reviewed the manuscript.

Funding: The work was supported by the National Natural Science Foundation of China (Nos. U20A2092, 42002106, 41907262 and 41502089), the Central Public Welfare Scientific Research Basic Scientific Research Business Expenses (No. KK2005), the National Basic Research Program of China (973 program) (No. 2011CB403007) and the China Geological Survey (No. DD20190606). We are grateful to reviewers for their Critical and constructive review.

Conflicts of Interest: The authors declare no competing interests.

Additional information: Correspondence and requests for materials should be addressed to C.L.W.

References

1. Abels, H.A.; Lauretano, V.; Yperen, A.V.; Hopman, T.; Zachos, J.C.; Lourens, L.J.; Gingerich, P.D.; Bowen, G.J. Carbon isotope excursions in paleosol carbonate marking five early Eocene hyperthermals in the Bighorn Basin, Wyoming. *Clim. Past* 2015, 11, 1857-1885.
2. Bhatia, M.R.; Crook, K.A. Trace element characteristics of graywackes and tectonic setting discrimination of sedimentary basins. *Contrib. Mineral. Petrol.* 1986, 92, 181-193.
3. Boynton, W.V. Geochemistry of the rare earth elements: Meteorite studies. In *Developments in Geochemistry*; Henderson, P., Ed.; Elsevier, 1984; pp. 63-114.
4. Cao, J.; Wu, M.; Chen, Y.; Hu, K.; Bian, L.Z; Wang, L.G.; Zhang, Y. Trace and rare earth elements geochemistry of Jurassic mudstones in the northern Qaidam basin, northwest China. *Chem. Erde-Geochem.* 2012, 72, 245-252.
5. Chen, W.T.; Zhou, M.; Zhao, X. Late Paleoproterozoic sedimentary and mafic rocks in the Hekou area, SW China: Implication for the reconstruction of the Yangtze Block in Columbia. *Precambrian Res.* 2013, 231, 61-77.
6. Chen, Z.L.; Ding, Z.L.; Tang, Z.H.; Wang, X.; Yang, S.L. Early Eocene carbon isotope excursions: Evidence from the terrestrial coal seam in the Fushun Basin, Northeast China. *Geophys. Res. Lett.* 2014, 41, 3559-3564.
7. Dai, S.W. Discussion on the regional structural features of Jianghan Basin since the indosinian movement. *J. Geomech.* 1996, 04, 82-86.
8. Fang, C.G.; Zhang, C.C.; Huang, N.; Teng, L.; Li, C.H.; Shao, W.; Zeng, M. Geological significance of rare earth elements in marine shale of the upper Permian Dalong Formation in the lower Yangtze region, south China. *Minerals* 2023, 1195.
9. Fedo, C.M.; Nesbitt, H.W.; Young, G.M. Unraveling the effects of potassium metasomatism in sedimentary rocks and paleosoils, with implications for paleoweathering conditions and provenance. *Geology* 1995, 23, 921-924.
10. Fu, X.G.; Wang, J.; Chen, W.B.; Feng, X.L.; Wang, D.; Song, C.Y.; Zeng, S.Q.. Elemental geochemistry of the early Jurassic black shales in the Qiangtang Basin, eastern Tethys: constraints for palaeoenvironment conditions. *Geol. J.* 2016, 51, 443-454.

11. Gilder, S.A.; Keller, G.R.; Luo, M.; Goodell, P.C. Timing and spatial distribution of rifting in China. *Tectonophysics* 1991, 197, 225-243.
12. Guo, Z.T.; Sun, B.; Zhang, Z.S.; Peng, S.Z.; Xiao, G.Q.; Ge, J.Y.; Hao, Q.Z.; Qiao, Y.S.; Liang, M.Y.; Liu, J.F.; Yin, Q.Z.; Wei, J.J. A major reorganization of Asian climate by the early Miocene. *Clim. Past* 2008, 4, 153-174.
13. Harnois, L. The CIW index: a new chemical index of weathering. *Sediment. Geol.* 1988, 55, 319-322.
14. Hasegawa, H.; Tada, R.; Jiang, X.; Suganuma, Y.; Imsamut, S.; Charusiri, P.; Ichinnorov, N.; Khand, Y.. Drastic shrinking of the Hadley circulation during the mid-Cretaceous Supergreenhouse. *Clim. Past* 2012, 8, 1323-1337.
15. Hetzel, A.; März, C.; Vogt, C.; Brumsack, H.J. Geochemical environment of Cenomanian-Turonian black shale deposition at Wunstorf (northern Germany). *Cretaceous Res.* 2011, 32, 480-494.
16. Hu, S.; Raza, A.; Min, K.; Kohn, B.P.; Reiners, P.W.; Ketcham, R.A.; Wang, J.; Gleadow, A.J.W. Late Mesozoic and Cenozoic thermotectonic evolution along a transect from the north China craton through the Qinling orogen into the Yangtze craton, central China. *Tectonics* 2006, 25, TC6009.
17. Jia, J.L.; Liu, Z.J.; Bechtel, A.; Strobl, S.A.I.; Sun, P.C. Tectonic and climate control of oil shale deposition in the Upper Cretaceous Qingshankou Formation (Songliao Basin, NE China). *Int. J. Earth Sci.* 2013, 102, 1717-1734.
18. Johanson, C.M.; Fu, Q. Hadley cell widening: model simulations versus observation. *J. Clim.* 2009, 22, 2713-2725.
19. Johnsson, M.J. The system controlling the composition of clastic sediments. *Geol. Soc. Amer. Spec. Pap.* 1993, 284, 1-19.
20. Jones, B.; Manning, D.A.C. Comparison of geochemical indices used for the interpretation of palaeoredox conditions in ancient mudstones. *Chem. Geol.* 1994, 111, 111-129.
21. Li, H.N.; Wang, C.L.; Liu, C.L.; Yang, S.G., Xu, H.M.; Yu, X.C.; Hu, H.B. A research on early Eocene homogenization temperature of fluid inclusions in halite and its paleoclimatic significance in Jiangling depression. *Miner. Deposits (Beijing, China)* 2016, 35, 1205-1216.
22. Li, H.N.; Wang, C.L.; Liu, C.L.; Yang, S.G.; Xu, H.M.; Hu, H.B.; Yu, X.C.; Liu, J.L. Paleotemperatures of Early Eocene in the Jiangling depression: Evidence from fluid inclusions in thenardite. *Acta Geol. Sin.* 2015, 89, 2019-2027.
23. Li, W.; Lu, S.; Xue, H.; Zhang, P.; Wu, S. The formation environment and developmental models of argillaceous dolomite in the Xingouzui Formation, the Jianghan Basin. *Mar. Pet. Geol.* 2015, 67, 692-700.
24. Li, X.Y.; Zhu, P.M.; Kusky, T.M.; Gu, Y.; Peng, S.B.; Yuan, Y.F.; Fu, J.M. Has the Yangtze craton lost its root? A comparison between the North China and Yangtze cratons. *Tectonophysics* 2015, 655, 1-14.
25. Liu, C.L. Characteristics and formation of potash deposits in continental rift basins: a review. *Acta Geosci. Sin.* 2013, 34, 515-527.
26. Liu, C.L.; Yu, X.C.; Zhao, Y.J.; Wang, J.Y.; Wang, L.C.; Xu, H.M.; Li, J.; Wang, C.L. A tentative discussion on regional metallogenic background and mineralization mechanism of subterranean brines rich in potassium and lithium in south China block. *Miner. Deposits (Beijing, China)* 2016, 35, 1119-1143.
27. Liu, C.L.; Zhao, Y.J.; Fang, X.M.; Lv, F.L.; Wang, L.C.; Yan, M.D.; Zhang, H.; Ding, T. Plate tectonic control on the distribution and formation of the marine potash deposits. *Acta Geol. Sin. (Chin. Ed.)* 2015, 89, 1893-1907.
28. Liu, M.; Cui, X.J.; Liu, F.T. Cenozoic rifting and volcanism in eastern China: a mantle dynamic link to the Indo-Asian collision? *Tectonophysics* 2004, 393, 29-42.
29. Lu, J.; Vecchi, G.A.; Reichler, T. Expansion of Hadley cell under global warming. *Geophys. Res. Lett.* 2007, 34, L06805.
30. McLennan, S.M. Rare earth elements in sedimentary rocks: influence of provenance and sedimentary processes. *Rev. Mineral. Geochem.* 1989, 21, 169-200.
31. McLennan, S.M.; Hemming, S.; McDaniel, D.K.; Hanson, G.N. Geochemical approaches to sedimentation, provenance, and tectonics. *Spec. Pap. - Geol. Soc. Am.* 1993, 284, 21-40.
32. McLennan, S.M.; Hemming, S.R.; Taylor, S.R.; Eriksson, K.A. Early Proterozoic crustal evolution: geochemical and Nd-Pb isotopic evidence from metasedimentary rocks, southwestern North America. *Geochim. Cosmochim. Acta* 1995, 59, 1153-1177.
33. Meng, Q.T.; Liu, Z.J.; Bruch, A.A.; Liu, R.; Hu, F. Palaeoclimatic evolution during Eocene and its influence on oil shale mineralisation, Fushun Basin, China. *J. Asian Earth Sci.* 2012, 45, 95-105.
34. Middelburg, J.J.; Van der Weijden, C.H.; Woittiez, J.R.W. Chemical processes affecting the mobility of major, minor and trace elements during weathering of granitic rocks. *Chem. Geol.* 1988, 68, 253-273.
35. Nesbitt, H.W.; Young, G.M. Early Proterozoic climates and plate motions inferred from major element chemistry of lutites. *Nature* 1982, 299, 715-717.
36. Nesbitt, H.W.; Young, G.M. Prediction of some weathering trends of plutonic and volcanic-rocks based on thermodynamic and kinetic considerations. *Geochim. Cosmochim. Acta* 1984, 48, 1523-1534.

37. Samanta, A.; Bera, M.K.; Ghosh, R.; Bera, S.; Filley, T.; Pande, K.; Rathore, S.S.; Rai, J.; Sarkar, A. Do the large carbon isotopic excursions in terrestrial organic matter across Paleocene-Eocene boundary in India indicate intensification of tropical precipitation? *Palaeogeogr. Palaeoclimatol. Palaeoecol.* 2013, 387, 91-103.
38. Shen, C.B.; Donelick, R.A.; O'Sullivan, P.B.; Jonckheere, R.; Yang, Z.; She, Z.B.; Miu, X.L.; Ge, X. Provenance and hinterland exhumation from LA-ICP-MS zircon U-Pb and fission-track double dating of Cretaceous sediments in the Jianghan Basin, Yangtze block, central China. *Sediment. Geol.* 2012, 281, 194-207.
39. Shen, L.J.; Liu, C.L.; Xu, H.M.; Wang, C.L.; Wang, L.C.; Liu, B.K.; Zhang, L.B. Paleocene mineral assemblage characteristics of Jianghan depression and their significance for potash formation. *Miner. Deposits (Beijing, China)* 2014, 33, 1020-1030.
40. Shu, L.S.; Faure, M.; Wang, B.; Zhou, X.M.; Song, B. Late Palaeozoic-Early Mesozoic geological features of South China: Response to the Indosinian collision events in Southeast Asia. *C. R. Geosci.* 2008, 340, 151-165.
41. Sun, X.J.; Wang, P.X.. How old is the Asian monsoon system? Palaeobotanical records from China. *Palaeogeogr. Palaeoclimatol. Palaeoecol.* 2005, 222, 181-222.
42. Taylor, S.R.; McLennan, S.M. The Continental Crust: Its Composition and Evolution. *J. Geol.* 1985, 94, 57-72.
43. Teng, X.H.; Fang, X.M.; Kaufman, A.J.; Liu, C.L.; Wang, J.Y.; Zan, J.B.; Yang, Y.B.; Wang, C.L.; Xu, H.M.; Schulte, R.F.; Piatak, N.M. Sedimentological and mineralogical records from drill core SKD1 in the Jianghan Basin, Central China, and their implications for late Cretaceous-early Eocene climate change. *J. Asian Earth Sci.* 2019, 182, 103936.1-103936.14.
44. Teng, X.H.; Wang, C.L.; Liu, C.L.; Yan, K.; Luo, Z. Paleocene-Eocene Thermal Maximum lacustrine sediments in deep drill core SKD1 in the Jianghan Basin: a record of enhanced precipitation in central China. *Glob. Planet. Change* 2021, 205, 103620.
45. Tribovillard, N.; Algeo, T.J.; Lyons, T.; Riboulleau, A. Trace metals as paleoredox and paleoproductivity proxies: An update. *Chem. Geol.* 2006, 232, 12-32.
46. Wanas, H.A.; Assal, E.M. Provenance, tectonic setting and source area-paleoweathering of sandstones of the Bahariya Formation in the Bahariya Oasis, Egypt: An implication to paleoclimate and paleogeography of the southern Neo-Tethys region during Early Cenomanian. *Sediment. Geol.* 2020, 413, 105822.
47. Wang, C.L.; Liu, C.L.; Wang, J.Y.; Yu, X.C.; Yan, K. Palynology and stratigraphy of the thick evaporate-bearing Shashi Formation in Jiangling Depression, Jianghan Basin of South China, and its paleoclimate change. *China Geol.* 2020, 2, 283-291.
48. Wang, C.L.; Liu, C.L.; Xu, H.M.; Wang, L.C.; Zhang, L.B. Carbon and oxygen isotopes characteristics of Paleocene saline lake facies carbonates in Jiangling depression and their environmental significance. *Acta Geosci. Sin.* 2013, 34, 567-576.
49. Wang, C.L.; Yan, K.; Yu, X.C.; Wang, J.Y.; Liu, D.H.; Shen, L.J; Li, R.Q.; You, C. ^{40}Ar/39Ar Geochronology, Geochemistry and Petrogenesis of the Volcanic Rocks in the Jiangling Basin, China. *Minerals* 2022, 12, 1099.
50. Wang, C.L.; Yu, X.C.; Li, R.Q.; Yan, K.; You, C. Origin of lithium-potassium brines in the Jianghan Basin, South China: constraints by water-rock reactions of Mesozoic-Cenozoic igneous rocks. *Minerals* 2021, 11, 1330.
51. Worash, G. Geochemistry provenance and tectonic setting of the Adigrat sandstone northern Ethiopia. *J. Afr. Earth Sci.* 2002, 35, 185-198.
52. Wu, L.L.; Mei, L.F.; Liu, Y.S.; Luo, J.; Min, C.Z.; Lu, S.L.; Li, M.H.; Guo, L.B. Multiple provenance of rift sediments in the composite basin-mountain system: constraints from detrital Zircon U-Pb geochronology and heavy minerals of the early Eocene Jianghan Basin, Central China. *Sediment. Geol.* 2017, 349, 46-61.
53. Xie, Y.L.; Wu, F.L.; Fang, X.M. A transient south subtropical forest ecosystem in central China driven by rapid global warming during the Paleocene-Eocene Thermal Maximum. *Gondwana Res.* 2022, 101, 192-202.
54. Yan, K.; Wang, C.L.; Liu, C.L.; Mischke, S.; Wang, J.Y.; Yu, X.C. Reconstruction of early Paleogene landscapes and climate in the Jianghan Basin, central China: Evidence from evaporates and palynology. *Palaeogeogr. Palaeoclimatol. Palaeoecol.* 2022, 601, 111095.
55. Yang, C.Q.; Chen, K.Q.; Cheng, Z.Q.; Zhan, H.J. Constituent evolution and exploration potential in Jianghan depression. *Nat. Gas Ind.* 2003, 23, 51-54.
56. Yao, W.H.; Li, Z.X.; Li, W.X.; Su, L.; Yang, J.H. Detrital provenance evolution of the Ediacaran-Silurian Nanhua foreland basin, South China. *Gondwana Res.* 2015, 28, 1449-1465.
57. Yu, X.C.; Liu, C.L.; Wang, C.L.; Wang, J.Y.; Xu, H.M.; Li, H.N. Sedimentary characteristics and palaeoclimatic significance of glauberite in Paleocene lacustrine deposits of the Jiangling depression, central China. *Geosci. J.* 2018, 22, 1-16.
58. Yu, X.C.; Liu, C.L.; Wang, C.L.; Xu, H.M. Provenance of rift sediments in a composite basin-mountain system: constraints from petrography, whole-rock geochemistry, and detrital zircon U-Pb geochronology of the Paleocene Shashi Formation, southwestern Jianghan Basin, central China. *Int. J. Earth Sci.* 2018, 107, 1-26.
59. Yu, X.Q.; Shu, L.S.; Deng, P.; Wang, B.; Zu, F.P. The sedimentary features of the Jurassic-Tertiary terrestrial strata in southeast China. *J. Stratigr.* 2003, 27, 224-263.

60. Zhang, T.F.; Sun, L.X.; Zhang, Y.; Cheng, Y.H.; Li, Y.F.; Ma, H.L.; Lu, C.; Yang, C.; Guo, G.W. Geochemical characteristics of the Jurassic Yan'an and Zhiluo Formations in the northern margin of Ordos Basin and their paleoenvironmental implications. *Acta Geol. Sin.* 2016, 90, 3454-3472.
61. Zhao, Z.Y.; Zhao, J.H.; Wang, H.J.; Liao, J.D.; Liu, C.M. Distribution characteristics and applications of trace elements in Junggar Basin. *Nat. Gas Explor. Dev.* 2007, 30, 30-33.